PNAS RESEARCH ARTICLE | NEUROSCIENCE

Sensory tuning in neuronal movement commands

Matthias P. Baumann[a,b,1], Amarender R. Bogadhi[a,b,c,1], Anna F. Denninger[a,b], and Ziad M. Hafed[a,b,2]

Edited by Stephen Lisberger, Duke University School of Medicine, Durham, NC; received April 10, 2023; accepted August 2, 2023

Movement control is critical for successful interaction with our environment. However, movement does not occur in complete isolation of sensation, and this is particularly true of eye movements. Here, we show that the neuronal eye movement commands emitted by the superior colliculus (SC), a structure classically associated with oculomotor control, encompass a robust visual sensory representation of eye movement targets. Thus, similar saccades toward different images are associated with different saccade-related "motor" bursts. Such sensory tuning in SC saccade motor commands appeared for all image manipulations that we tested, from simple visual features to real-life object images, and it was also strongest in the most motor neurons in the deeper collicular layers. Visual-feature discrimination performance in the motor commands was also stronger than in visual responses. Comparing SC motor command feature discrimination performance to that in the primary visual cortex during steady-state gaze fixation revealed that collicular motor bursts possess a reliable perisaccadic sensory representation of the peripheral saccade target's visual appearance, exactly when retinal input is expected to be most uncertain. Our results demonstrate that SC neuronal movement commands likely serve a fundamentally sensory function.

active vision | superior colliculus | saccades | perisaccadic perception | perceptual stability

Besides supporting a broad range of cognitive functions (1), the superior colliculus (SC) plays a fundamental role in oculomotor control (2, 3). It issues saccade motor commands in the form of perimovement "motor" bursts time-locked to movement onset (4–6). Such bursts specify saccade metrics (direction and amplitude) via a distributed place code of bursting neurons (7), and they are also widely believed to determine saccade kinematics, such as speed (8), via a rate code within the bursts themselves. However, practically all models of saccade control by the SC rely on observations with small light spots as the saccade targets (Fig. 1 *A* and *B*). Instead, in natural behavior, we generate eye movements toward image features, such as faces, cars, or trees.

If SC movement-related motor bursts were purely a neuronal control signal (8–11), then similar saccades to different visual images should yield similar motor bursts. We tested this by training monkeys to generate saccades toward different image patches. The patches were always placed within the movement-related response field (mRF) of a recorded neuron, thus being associated with strong motor bursts. When we modified the visual features of the image patches, we also strongly modified the SC motor bursts and for a wide range of visual image features. This modification, which also differentiated between coherent and scrambled images of real-life objects, was the outcome of a transformed representation of the peripheral saccade target visual appearance at the time of eye movement triggering. Our results document a potential neuronal mechanism for bridging the transsaccadic period of maximal sensory uncertainty caused by rapid saccade-induced retinal image shifts, and they help account for a wide range of well-known perisaccadic alterations in visual perception.

Results

Saccade Motor Bursts Are Sensory Tuned. Consider the example neuron of Fig. 1*C*. When tested classically with a spot as the saccade target, it exhibited practically no visual sensitivity at stimulus onset (Fig. 1 *C*, *Top*), but it was clearly motor related (Fig. 1 *C*, *Bottom*): It emitted a strong burst of action potentials time-locked to eye movement triggering. In Fig. 1*D*, we presented a grating inside the same neuron's mRF, and we measured saccade-related motor bursts. In one example manipulation, we randomly varied the spatial frequency of the target across trials, and in another, we altered its contrast; in a third manipulation, we varied orientation. We always ensured that within each image manipulation, the generated saccades were behaviorally matched across the different images serving as the saccade targets (Fig. 1*E*; an example from the spatial frequency manipulation is shown; *Materials and Methods*). In every case, the neuron's

Significance

The superior colliculus (SC) triggers rapid orienting gaze shifts, called saccades, via strong movement-locked "motor" bursts. We show that these bursts are strongly detached from direct motor control and are instead visual-feature tuned, changing in their properties for different eye-movement target images (despite similar movements). Such visual feature tuning of SC motor commands is not haphazard, being most prominent for coherent real-life object images as the eye movement targets, as opposed to featureless pictures, and also being strongest in the SC's most motor neurons. Our results suggest that the SC can relay, via re-entrant projections to the visual system, an internal estimate of peripheral saccade target appearance exactly when retinal image signals are most unreliable due to rapid eyeball rotations.

Author affiliations: [a]Physiology of Active Vision Laboratory, Werner Reichardt Centre for Integrative Neuroscience, Tübingen University, Tübingen 72076, Germany; [b]Hertie Institute for Clinical Brain Research, Tübingen University, Tübingen 72076, Germany; and [c]Central Nervous Systems Diseases Research, Boehringer Ingelheim Pharma GmbH & Co. KG, Biberach 88400, Germany

Author contributions: M.P.B., A.R.B., A.F.D., and Z.M.H. designed research; performed research; analyzed data; and wrote the paper.

The authors declare no competing interest.

This article is a PNAS Direct Submission.

[1]M.P.B. and A.R.B. contributed equally to this work.

[2]To whom correspondence may be addressed. Email: ziad.m.hafed@cin.uni-tuebingen.de.

This article contains supporting information online at https://www.pnas.org/lookup/suppl/doi:10.1073/pnas.2305759120/-/DCSupplemental.

Published September 11, 2023.

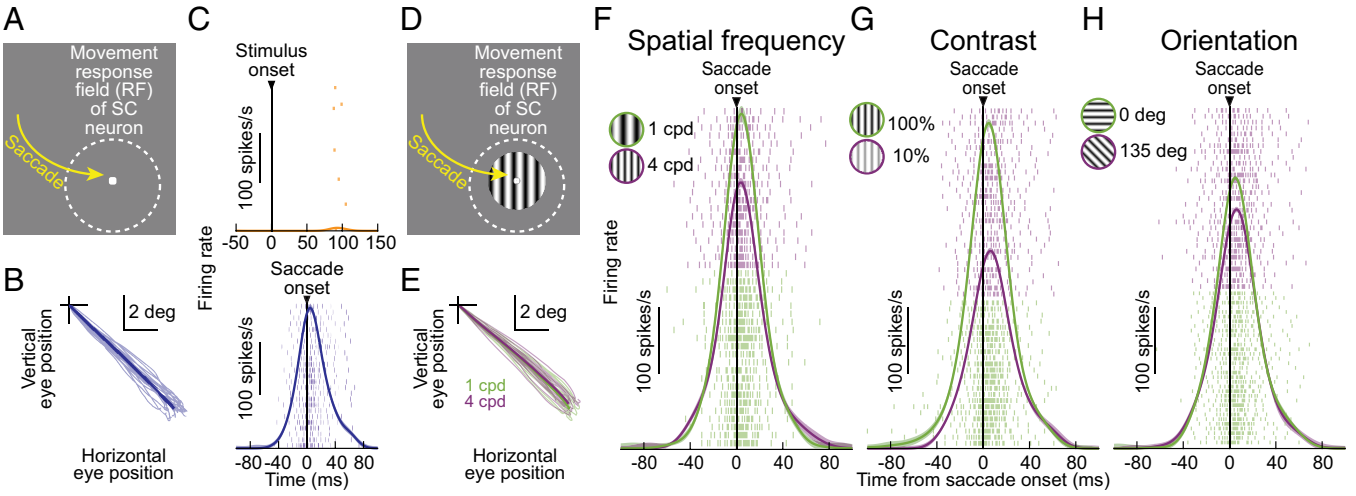

Fig. 1. Sensory tuning in SC neuronal movement commands. (*A*) A light spot was placed within the movement-related response field of a neuron. (*B*) Individual saccade vectors and their average (saturated line). (*C*) Stimulus-aligned (*Top*) and saccade-aligned (*Bottom*) firing rates from the neuron. Rasters show spike times across individual trial repetitions. The neuron exhibited practically no visual response but a strong movement-related burst. (*D*) The saccade target was now a grating. (*E*) Individual saccade vectors to a 1 cpd (green) or 4 cpd grating (purple) and their averages. The saccades were matched across different images. (*F*) Nonetheless, the motor bursts of the same neuron were different for different images. (*G* and *H*) Similar results when we manipulated target image contrast (*G*) or orientation (*H*). Error bars indicate 95% CIs, and numbers of trials are conveyed by the rows in the spike rasters.

movement-related motor bursts were different for different images (Fig. 1 *F*–*H*). This occurred even though the neuron itself was not particularly visually sensitive (Fig. 1*C*) and also despite the vector-matched saccades (Fig. 1*E*). Thus, this example neuron's motor bursts contained information about the visual appearance of the saccade target.

Similar observations held across our entire neuronal population and for all image manipulations that we tested (including contrasts, spatial frequencies, orientations, and bright-versus-dark luminance contrast polarities; also see Fig. 4 below for real-life visual object images). To summarize such sensory tuning in SC neuronal movement commands, we identified, for each neuron, the image associated with the strongest (most preferred visual feature) or weakest (least preferred visual feature) motor burst. In every image manipulation, the difference in motor bursts between the most and least preferred image features (expectedly always present by the definition of this analysis) was large, despite the matched saccades (Fig. 2*A*). In Fig. 2*B*, we also plotted raw perisaccadic neuronal firing rates in each shown image manipulation. Even though we know that SC motor bursts can be dissociated from movement kinematics (12, 13), we also confirmed that this difference in SC motor bursts was not trivially explained by equally large differences in eye movement kinematics. We did so by plotting saccade peak velocity (Fig. 2*C*) from the very same trials as in Fig. 2 *A* and *B*: The impact of the most and least preferred trial classification on the firing rates was much larger than that on movement kinematics. We also calculated a neuronal and a kinematic modulation index for each neuron and its recorded saccades; the index was zero if there were no differences between the most and least preferred trials (*Materials and Methods*). Neuronally, the modulation index was strongly skewed away from zero (Fig. 2*D*), but it straddled zero kinematically (Fig. 2*E*). Fig. 2*F* also plots the modulation indices against each other, showing that they were not correlated [P = 0.511, 0.059, 0.341, 0.064 in the spatial frequency, contrast, orientation, and luminance polarity manipulations, respectively; Pearson correlations: r(322) = −0.037, r(318) = 0.106, r(305) = 0.055, r(239) = −0.12]. Thus, sensory tuning in SC motor bursts (Figs. 1 and 2) was not explained by eye movement kinematics.

Naturally, the SC's population code (7) can also alter SC motor bursts. For example, a slightly deviated saccade vector for one image could be associated with an altered neuronal response, simply by activating a different portion of a given neuron's mRF. We minimized this by a clear marker at the center of every image (e.g., Fig. 1*D*; *Materials and Methods*), to better guide saccades. More importantly, we also performed post hoc vector matching of the saccades before analyzing the motor bursts, removing any outlier eye movement vectors (*Materials and Methods*; see Fig. 1*E*). To confirm the effectiveness of such vector matching, we tested saccade metrics in the accepted trials. For each neuron, and for the very same trials as in Fig. 2, we plotted saccade amplitude and direction errors, as well as their differences, for the most and least preferred images. The results, shown in *SI Appendix*, Fig. S1, confirm that saccade metric differences do not trivially explain the large SC motor burst differences of Figs. 1 and 2.

We also entertained the possibility that subsequent corrective saccades, sometimes called catch-up saccades, might have been different for different images. That is, we checked whether the different motor bursts that we observed for different images were associated with altered motor drives for the subsequent corrective movements. While this is unlikely, since corrective saccades are typically smaller than the primary saccades and therefore recruit different groups of SC neurons, we measured the onset time, amplitude, peak velocity, and direction of the first catch-up saccade to occur after the primary movement. We then plotted these distributions for the different feature exemplars within each of our image manipulations. Once again, there were no clear differences in catch-up saccade properties (*SI Appendix*, Fig. S2) despite the clear neuronal differences in the motor burst strengths.

It might additionally be argued that the intrinsic salience of individual image features might have introduced an internal reward signal (14, 15) associated with some saccade targets versus others. However, reward expectation affects both SC activity (16) (globally, including visual bursts, delay-period activity, and motor bursts) and the eye movement properties themselves (14), whereas we saw minimal kinematic alterations with large neuronal effects (Fig. 2 and *SI Appendix*, Fig. S1; also see refs. 12 and 13 for further evidence of dissociation between motor bursts and kinematics in other contexts). We also equalized the image conditions as much as possible, by associating all trials with the same rewards for the animal, and also by enforcing a time delay between stimulus onset

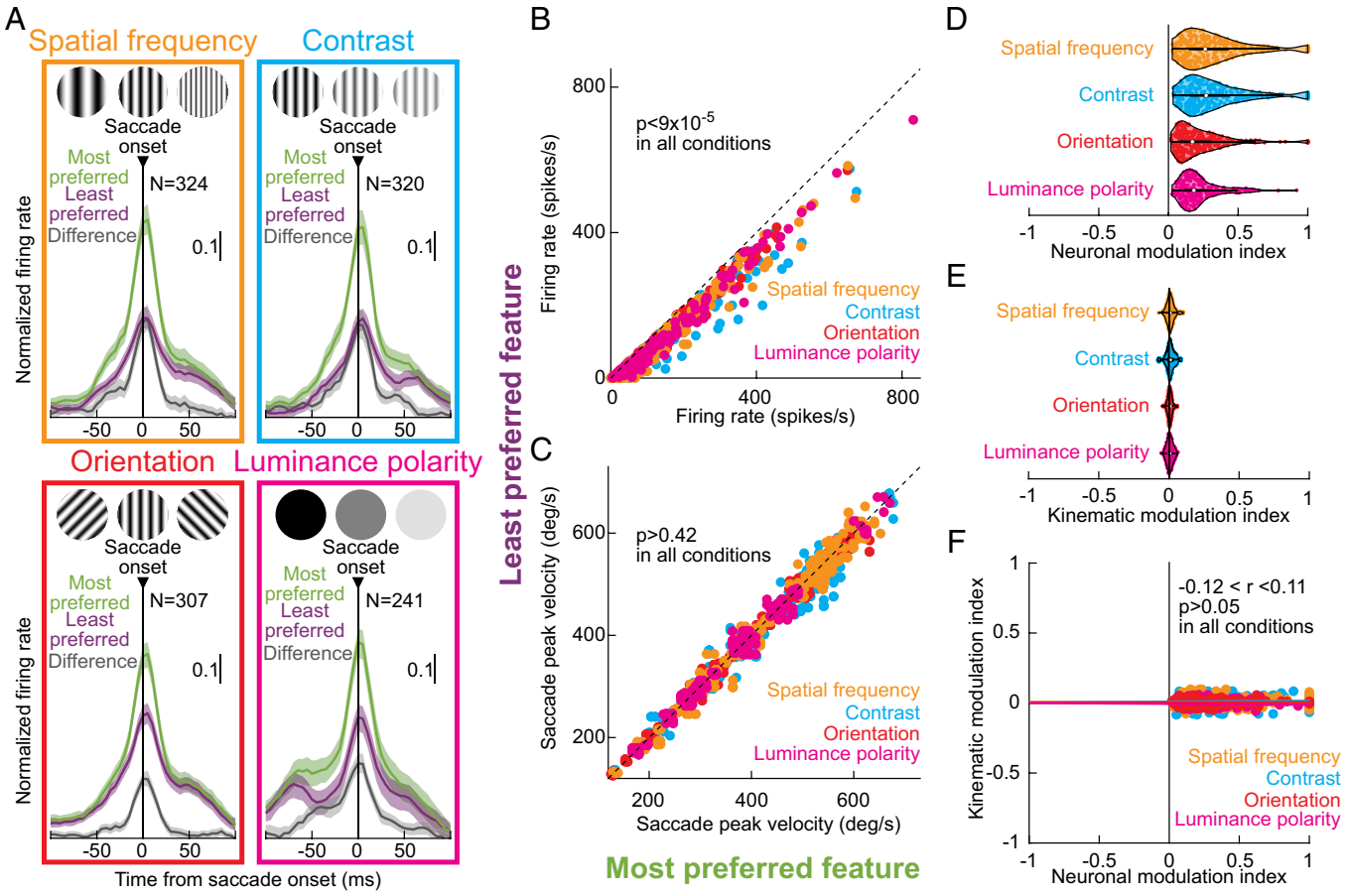

Fig. 2. Robustness of sensory tuning in SC neuronal movement commands across image manipulations. (*A*) Average normalized population firing rates for the most (green) and least (purple) preferred stimuli within each image manipulation and their differences (gray). In all cases, we observed a robust difference in SC motor bursts for different images. Note that for luminance polarity, the task was a reflexive visually guided saccade task. Thus, visual and motor bursts occurred in close temporal proximity, explaining secondary firing rate elevation at approximately −75 ms. Error bars indicate 95% CIs, and neuron numbers are indicated in each panel. (*B*) Individual neuron raw perisaccadic firing rates (−50 to 25 ms from movement onset; *Materials and Methods*) for most and least preferred targets, color-coded by each image manipulation as in *A*. (*C*) From the same trials as in *A* and *B*, saccade peak velocities were very similar for most and least preferred images, despite the large SC motor burst differences (*A* and *B*) (*P*-values indicate rank-sum test results in each image manipulation). (*D*) Violin plots of neuronal modulation indices between the most and least preferred features (*Materials and Methods*). Contrast and spatial frequency had the strongest neuronal effects. In each violin plot, the white circle indicates the median, and the thick bar indicates the interquartile range. (*E*) Kinematic modulation indices from the very same trials of each neuron. Despite the large neuronal modulations (*D*), the kinematic modulations straddled zero, consistent with *C*. (*F*) Neuronal and kinematic modulation indices were not correlated, suggesting that our results were not explained by differences in saccades for different images. *SI Appendix*, Fig. S1 also shows that other behavioral properties of saccades did not explain our neuronal results. Neuron numbers in *B*–*F* are the same as in *A*. Also see Fig. 4 showing sensory tuning in SC neuronal movement commands with real-life object images.

and the instruction to make a saccade (*Materials and Methods*). Besides ensuring a stable scene image at the time of saccade triggering, which is more similar to natural-looking behavior, this enforced delay reduced the impacts of potential differences in intrinsic image salience. For example, saccadic reaction time distributions were strongly overlapping for different spatial frequencies (*SI Appendix*, Fig. S3*A*), unlike what would happen with no enforced fixation (17, 18); similar results were also obtained in our other image manipulations (*SI Appendix*, Fig. S3 *B* and *C*), suggesting that potential intrinsic image salience did not explain the results of Figs. 1 and 2. Indeed, in one image manipulation (luminance polarity), we also explicitly skipped enforced fixation (*Materials and Methods*). Both example neurons (*SI Appendix*, Fig. S4 *A* and *B*) and the population (Fig. 2, luminance polarity data) revealed the same sensory tuning in SC neuronal movement commands even though saccadic reaction times were different across different conditions in this dataset (ref. 19 and *SI Appendix*, Fig. S4*C*). Therefore, whether stimuli were intrinsically salient (e.g., having low spatial frequency or high contrast) or not, sensory tuning in SC neuronal movement commands was still present. Our subsequent feature discrimination and population dynamic analyses, described in more detail below, will further demonstrate that different image orientations, which were of roughly equal visual salience across exemplars (when compared to our other tested feature sets), were still well differentiated in their associated SC motor bursts (e.g., see Fig. 3 *C* and *F* below and *SI Appendix*, Fig. S8 for more details).

Stronger Effect than in SC Visual Bursts. To quantitatively test discrimination performance of the most and least preferred image features from the visual or motor bursts of individual SC neurons, we used area under the ROC (receiver-operating-characteristic) curve (AUC) analyses (*Materials and Methods*), like in visual cortical presaccadic analyses (21). In Fig. 3 *A*–*C*, *Left*, we calculated the AUC at every time bin relative to stimulus onset, comparing a neuron's distribution of firing rates for most and least preferred images during steady-state gaze fixation. We defined the most and least preferred images in the visual bursts similarly to how we defined them for motor bursts: The most or least preferred image was that evoking the strongest or weakest visual response by a neuron, respectively (*Materials and Methods*; raw population firing rates are shown in *SI Appendix*, Fig. S5,

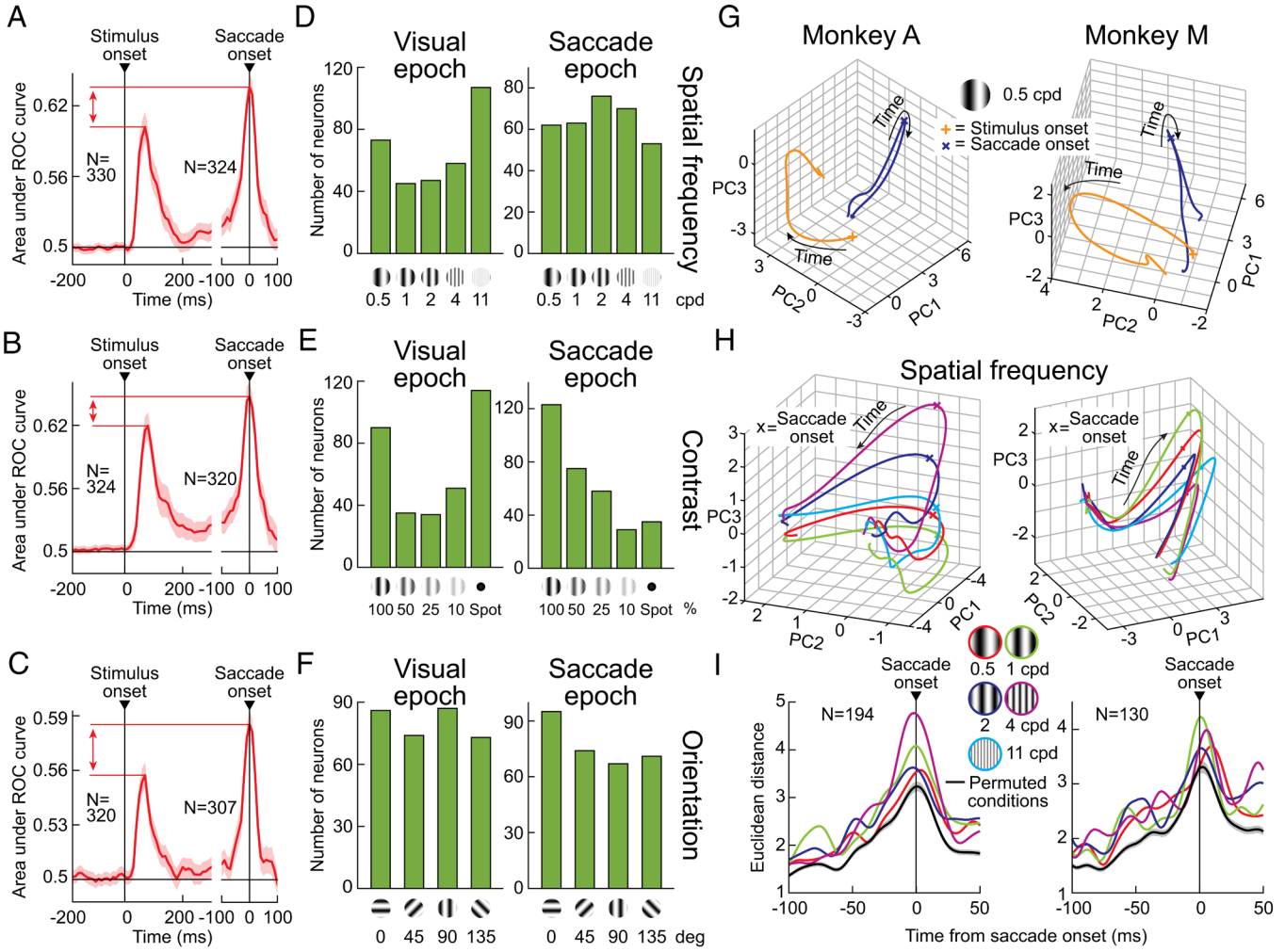

Fig. 3. Transformation of the visual sensory representation of saccade targets in the SC at the time of eye movement generation. (*A–C*) AUC discrimination performance between the most and least preferred images as a function of time from stimulus or saccade onset: (*A*) spatial frequency; (*B*) contrast; (*C*) orientation. In each case, it was possible to better discriminate between the most and least preferred images from the motor than visual bursts of individual SC neurons (vertical red arrows). Error bars indicate 95% CIs across neurons; neuron numbers are indicated in each panel. Note that for saccade burst analyses, we sometimes excluded a small number of neurons if there were not enough vector-matched movements across all image conditions of a given manipulation (*Materials and Methods*). This explains the small difference in neuron numbers between visual and motor burst epochs. (*D–F*) In each image manipulation, distribution of preferred features in the initial visual response (left column; visual epoch) or in saccade motor bursts (right column; saccade epoch). Sensory tuning in SC neuronal movement commands increased representation of visual features that were not normally preferred in visual epochs. (*G*) For an example image (0.5 cpd grating), trajectory of each monkey's entire population of neurons' firing rates after stimulus onset (orange; 0 to 200 ms) or perisaccadically (dark blue; −100 to 50 ms), after PCA dimensionality reduction (*Materials and Methods*). Perisaccadic population activity was more spatially constrained, consistent with recent evidence (20). Additionally, population activity occupied almost orthogonal manifolds in the visual and motor burst epochs, suggesting a transformed representation (*A–F*). (*H*) When we plotted the motor burst epochs (with higher zoom and a different view), but now for all the different spatial frequency images, the population trajectories were differentiated for each feature. Thus, it is possible for recipient neurons to read out information about saccade target visual appearance from SC motor bursts. (*I*) We picked a reference perisaccadic trajectory (11 cpd) in the high-dimensional population activity space of each monkey's neurons, and we then plotted Euclidean distances of population activity in each other image feature from this trajectory. For each image, Euclidean distances peaked at saccade onset (consistent with Figs. 1 and 2), and they were higher than distances obtained with randomly shuffled reference and nonreference trajectories (black ± 95% CIs). Thus, individual features were discriminable within SC motor bursts. *SI Appendix*, Figs. S8 and S9 show similar population analyses from all other image manipulations.

formatted similarly to Fig. 2). We only focused on the conditions enforcing a delay between stimulus onset and saccade generation, to avoid a temporal mixing between visual and motor bursts in reflexive saccade paradigms. In Fig. 3 *A–C*, *Right*, we performed the same analysis around saccade onset. In the visual epoch, there was an expected peak in the AUC value soon after stimulus onset; SC visual responses represent visual-scene image information (17, 22, 23). Critically, across the population, and in all image manipulations, there was also a strong perisaccadic peak in AUC discrimination performance, consistent with Figs. 1 and 2. This peak was at least as high as that in presaccadic elevations of visual cortical activity in area V4 (21). Thus, SC saccade motor bursts possess robust information about the visual appearance of the peripheral saccade target.

Intriguingly, we could better discriminate the most and least preferred images from SC motor rather than visual bursts (compare visual and motor epoch peaks in Fig. 3 *A–C*; error bars denote 95% CIs). These results likely represent a yet-to-be-appreciated underlying neuronal mechanism for well-known presaccadic enhancements of visual perception relative to steady-state gaze fixation (24–27).

It is also worth noting that a peak in perisaccadic AUC discrimination performance also clearly emerged in the reflexive saccade version of our tasks. Specifically, in this task, individual neurons preferred stimuli of different luminance polarity and contrast in their motor bursts (Fig. 2, luminance polarity data), with similar AUC discrimination performance levels as those seen in the other image manipulations (*SI Appendix*, Fig. S6*A*). We additionally

note here that this task did not have a small fixation marker in the middle of the presented images, as in the other tasks of Figs. 1–3. Yet, it still showed robust sensory tuning in the SC motor bursts (Fig. 2, luminance polarity data; *SI Appendix*, Figs. S4 and S6). Therefore, sensory tuning in SC neuronal movement commands still persisted for reflexive orienting responses.

Transformed Perisaccadic Scene Coding. Across all image manipulations shown so far, and irrespective of delayed or reflexive saccades, our results document a robust sensory signal embedded within SC motor bursts, which is not fully accounted for by saccade metric and kinematic properties, and which is at least as good as that present in initial visual sensory responses (and also in presaccadic visual cortical activity; ref. 21). We next investigated which image features individual neurons preferred.

In the visual burst epochs, we observed expected SC sensory tuning properties. For example, SC neuron visual bursts expectedly (17, 23, 28–30) preferred low spatial frequencies (Fig. 3*D*) and high contrasts (Fig. 3*E*), with the caveat being that the spot at each patch center (used to improve saccade vector matching; *Materials and Methods*) interacted with the underlying image patch, especially when the patch was least visible (e.g., having low contrast or high spatial frequency). The spot (introducing a broadband spatial frequency signal), therefore, changed the spectral and luminance content of the overall image, and this increased the numbers of neurons preferring high spatial frequencies or low contrasts in Fig. 3 *D* and *E* when compared to the literature (17, 23, 28–30). This, in itself further confirms that our neurons behaved as expected in their stimulus-evoked visual sensory responses (23).

Perisaccadically, all image features were well represented by the motor bursts (Fig. 3 *D–F*, saccade epoch). Critically, neurons often changed their preferred image features relative to the initial visual burst epoch (see example neurons in *SI Appendix*, Fig. S7). The result, across the population, was a transformed visual representation in the motor bursts, evidenced by different distributions of preferred image features across neurons (compare visual and saccade epochs in Fig. 3 *D–F*). For example, unlike in visual responses, mid-spatial frequencies became more prevalently represented in the motor bursts (Fig. 3*D*). This difference in feature preference from the visual burst epoch was statistically significant ($P = 4.8 \times 10^{-6}$; $\chi^2 = 30.0312$; χ^2 test comparing the two histograms). Similarly, for the contrast manipulation, lower contrasts (e.g., 25%) became preferred more often (Fig. 3*E*); again, the histograms of preferences across the visual and motor burst epochs were statistically significantly different from each other ($P = 3.5 \times 10^{-15}$; $\chi^2 = 73.8329$). Interestingly, in both of these cases, these results suggest that intrinsic salience on its own (e.g., low spatial frequency or high contrast) was not the sole factor determining SC motor burst strength in our experiments. This is because relatively more neurons actually preferred the "weaker" stimuli in their motor bursts than in their visual responses. For the orientation tuning task, the differences in histograms (Fig. 3*F*) were not statistically significant ($P = 0.2544$; $\chi^2 = 4.0663$), consistent with the fact that all orientations were already well represented to begin with in the visual burst epoch. Thus, overall, there was effectively a relative equalization of preferred features in the motor bursts: Images that were less likely to be preferred in visual bursts were more preferred during the motor commands.

The above transformation of visual information in the SC motor bursts is very interesting given that spatial frequency perception in humans increases its bandwidth (shifting toward higher spatial frequencies; like in Fig. 3*D*) presaccadically (27). Presaccadic contrast sensitivity is also enhanced (26, 29), consistent with the enhanced preferences for low contrasts in our SC motor bursts. In fact, in our reflexive saccade paradigm, we used a relatively smaller saccade target (as opposed to large gratings; *Materials and Methods*). Even in that case, a clear preference for high contrasts in the visual response epochs was transformed into one in which lower contrasts became better represented by the SC population at saccade triggering (*SI Appendix*, Fig. S6 *B* and *C*; also see the example neuron of *SI Appendix*, Fig. S4*B*). Therefore, the visual appearance of the saccade target is represented by SC motor bursts using a transformed code amplifying weak visual signals.

To further understand the transformation of visual target representations in SC motor bursts, we estimated the high-dimensional state-space trajectory (20) of our recorded neurons' activities either after stimulus onset or perisaccadically (*Materials and Methods*). We first created, for each time, a point in an N-dimensional space of N recorded neurons. For visualization purposes, we then performed principal components analysis (PCA) and plotted the three-dimensional trajectory of population activity using the first three principal components, which accounted for a great majority of the variance in the neuronal data (*Materials and Methods*). Prior work suggested that the population trajectory in the motor burst epoch should be relatively straight, compared to that in the visual burst epoch, suggesting a temporal alignment of the population at saccade triggering (20). We confirmed this (Fig. 3*G*). Critically, however, we uncovered two additional key properties of the SC population activity that are particularly relevant here.

First, there was an almost orthogonal relationship between population trajectory during the visual and motor burst epochs (Fig. 3*G*). Thus, areas reading out SC population activity encounter largely different state-space loci during fixation and saccades, consistent with the altered feature preferences of Fig. 3 *D–F*.

Second, when we repeated the same analyses around saccade onset, but now differentiating trials based on the different presented images, we confirmed the results of Figs. 1, 2, and 3 *A–F*: Perisaccadic population trajectory was different for different saccade target images, despite the matched vectors and kinematics across all spatial frequency conditions (Fig. 3*H*). To demonstrate that feature information was indeed present in the population during motor bursts, we then used one image feature [11 cpd (cycles per deg) in the example of Fig. 3*I*] as a reference high-dimensional population trajectory. Then, we calculated the Euclidean distance, at every time point, between each other feature condition (e.g., 4 cpd) and this reference condition. The Euclidean distance always peaked at motor burst time, and it was different for different image features (Fig. 3*I*). Moreover, all of the peak Euclidean distances were larger than those expected by random permutation of reference and condition trajectories (black line in Fig. 3*I*; *Materials and Methods*). *SI Appendix*, Fig. S8 shows how perisaccadic distances were consistently different for different images in our other image manipulations as well. Therefore, at the time of saccades, there was a graded, differentiated representation of visual image features by SC populations.

Visual Objects Are Also Well Represented. Since natural-looking behavior typically involves foveating specific objects, a strong test of the ecological relevance of sensory tuning in SC neuronal movement commands would be to check high-level visual object representations. We, therefore, studied motor bursts for luminance-equalized natural images of animate and inanimate objects, as well as feature- and spectral-scrambled versions of them (Fig. 4*A*; *Materials and Methods*). We recently found that SC visual responses are indeed sensitive to coherent visual object images (31), so we wondered whether this also held in the motor bursts.

The largest differences in SC motor burst strengths between the most and least preferred images occurred with such naturalistic

images. For example, Fig. 4*B* shows that the motor burst of an example neuron was almost completely abolished when making saccades toward a nonpreferred scrambled image. Across the population, there was a larger difference between preferred and least preferred images in this experiment than with simple feature dimensions (compare Fig. 4*B*, right to Fig. 2*A*), and AUC discrimination performance was also still higher during the motor bursts than during earlier visual bursts (Fig. 4*C*). These effects were, again, not explained by eye movement effects (Fig. 4 *D* and *E* and *SI Appendix*, Fig. S9 *A–C*).

Most interestingly, a majority of neurons had the most preferred image during saccade motor bursts as a real object image (first two columns in the histogram of Fig. 4 *F*, *Top*) and the least preferred image as a scramble (last two columns in the histogram of Fig. 4 *F*, *Bottom*). Individual SC neurons' motor bursts also contained significant information about whether a saccade target was a coherent or scrambled object image, as revealed by a significant peak in perisaccadic AUC discrimination performance in Fig. 4*G*. And, high-dimensional population trajectories in the motor burst epoch systematically differentiated between coherent and both types of scrambled object images (*SI Appendix*, Fig. S9 *D–G*).

Thus, sensory tuning in SC neuronal movement commands extended to high-level visual object representations. This suggests an ecological relevance of sensory tuning in SC neuronal movement commands in more naturalistic active vision scenarios.

Strongest Effect in Least Visual Neurons. Sensory tuning in SC neuronal movement commands was not restricted to a single functional cell type, but it was a robust property of all movement-related neurons. In fact, AUC discrimination performance was highest for the most motor neurons, occupying the deeper SC layers (5, 6) and typically having weak to nonexistent visual responses. We visualized this in each task (with dissociated visual and motor burst times) by repeating our AUC analyses of Fig. 3 *A–C*, but now after classifying how each neuron responded in either the visual or motor epoch of the task (*Materials and Methods*).

Fig. 5*A* shows example normalized population firing rates clarifying the different functional cell types in our database (*Materials and Methods*). In Fig. 5 *B–E*, we plotted AUC discrimination performance in either the visual or motor burst epochs across the different cell types. AUC discrimination performance in the motor bursts was always the highest for the most motor neurons. We first confirmed this by plotting, for each task (each row in Fig. 5 *B–E*), a horizontal dashed line marking the peak perisaccadic AUC discrimination performance in the most motor neurons (rightmost column) and extending this horizontal line leftward toward the

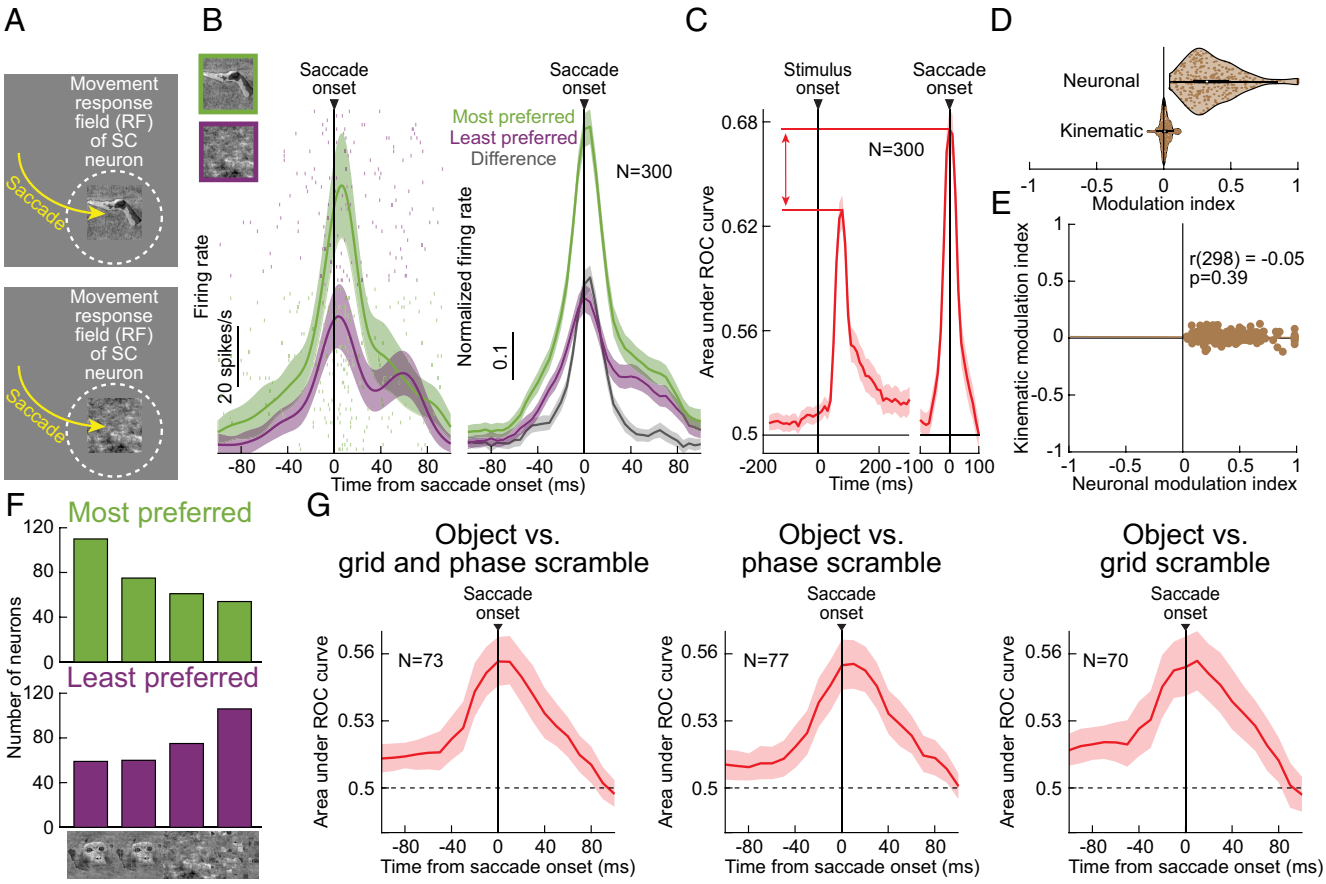

Fig. 4. Sensitivity of SC neuronal movement commands to coherent visual object images. (*A*) We tested saccades to real-life objects or their scrambles (31). (*B*) *Left*: Example neuron's saccade motor bursts for an image of a hand (green) or a phase-scrambled (31) version of it (purple); the neuron preferred the coherent image. *Right*: Across the population, most preferred images (green) had a much higher perisaccadic firing rate than least preferred images (purple), and the difference (gray) was larger than in our other image manipulations (compare to Fig. 2*A*). (*C*) Like in Fig. 3 *A–C*, AUC discrimination performance was higher in motor than visual bursts. (*D* and *E*) Moreover, there was no correlation between neuronal and kinematic modulation indices (as in Fig. 2 *D–F*). *SI Appendix*, Fig. S9 *A–C* shows additional controls for other saccade behavioral metrics. (*F*) In the SC motor bursts, the most preferred images were most likely to be coherent object images (first two columns; top histogram); the least preferred images were most likely to be scrambles (last two columns; bottom histogram). Also see *SI Appendix*, Fig. S9 *D–G* for further evidence from high-dimensional population state-space analyses. (*G*) Consistent with this, we found a substantial number of neurons with significant (*Materials and Methods*) AUC discrimination performance between real and scrambled images of different kinds in the saccade motor bursts. Thus, SC motor bursts are sensitive to real-life object images as saccade targets. Error bars: 95% CIs.

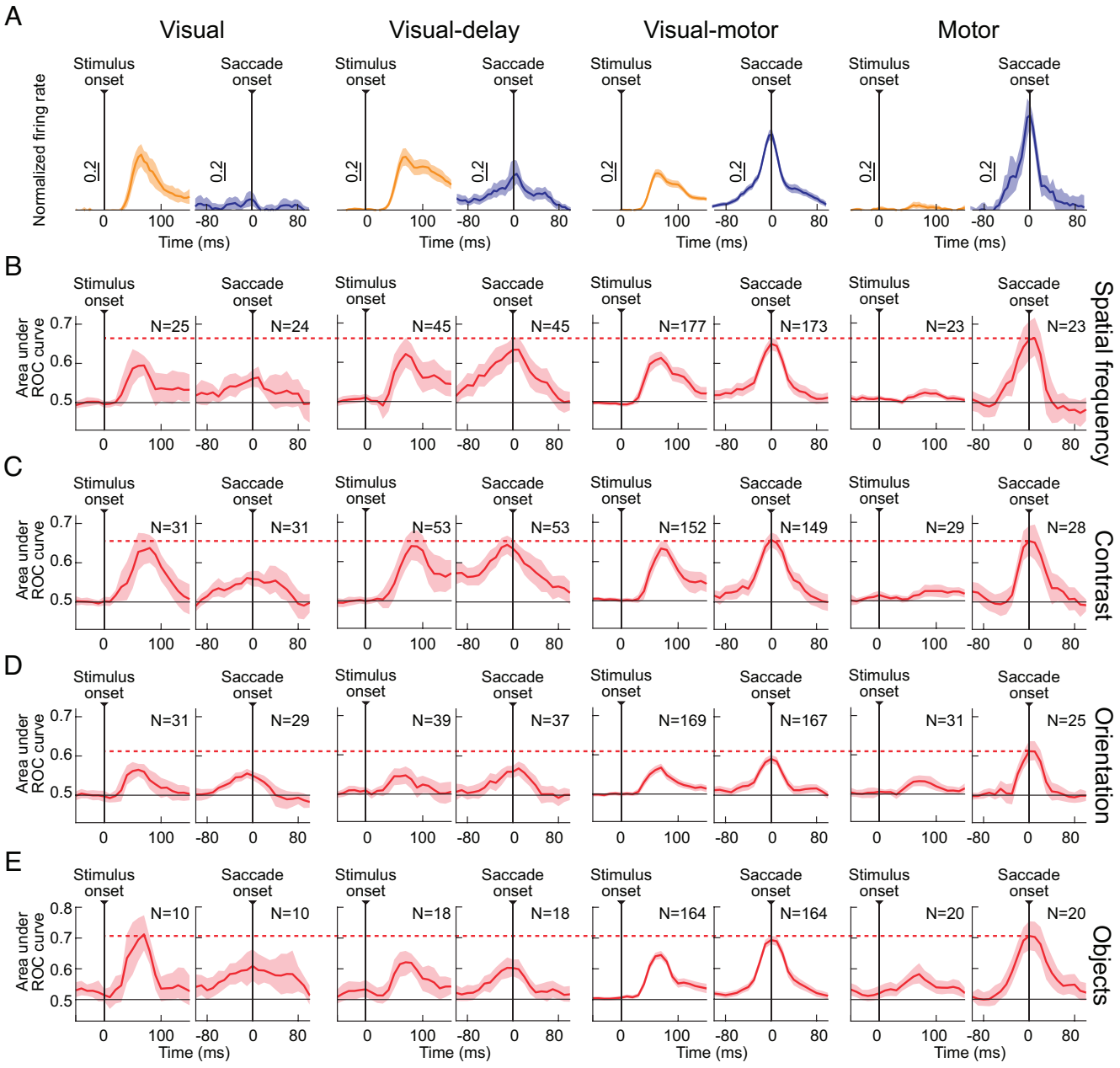

Fig. 5. Pervasiveness of sensory tuning in SC neuronal movement commands across movement-related cell types. (*A*) In each image manipulation, we classified neurons as visual (leftmost column), visual-delay (second column), visual-motor (third column), or motor (fourth column) based on their peristimulus, perisaccadic, or delay-period activity (*Materials and Methods*). The example shown is for the preferred conditions of the spatial frequency manipulation. (*B–E*) For each image manipulation, we plotted peristimulus or perisaccadic AUC discrimination performance (like in Figs. 3 and 4) but for each functionally identified cell type separately. Visual neurons had the weakest perisaccadic discrimination performance because they had weak or nonexistent motor bursts. However, for all other cell types, discrimination performance in the motor bursts was at least as good as, if not better, than discrimination performance in the visual bursts. Moreover, motor burst discrimination performance was the highest in each image manipulation for the most motor neurons (see the horizontal dashed line comparing motor neuron perisaccadic performance to the other cell types). Error bars: 95% CIs.

panels of the other functional cell types. As can be seen, no other SC functional cell type reached a higher level of motor burst AUC discrimination performance than the most motor neurons, and some functional cell types had clearly lower motor burst AUC discrimination performance.

We then measured AUC discrimination performance in the motor burst epochs by averaging across the interval ±20 ms from saccade onset (*Materials and Methods*), and we performed a Kruskal–Wallis nonparametric ANOVA across cell types. In each task, there was a significant effect of functional cell type on motor burst AUC discrimination performance ($P = 4.55 \times 10^{-5}$, 9.94×10^{-6}, 0.0025, 0.0004 for spatial frequency, contrast, orientation, and real-life objects, respectively); post hoc tests suggested that visual–motor and motor neurons consistently had higher perimovement AUC discrimination performance than visual and visual-delay neurons. We additionally note that motor neurons also showed sensory tuning in our reflexive saccade paradigm with smaller targets (see the example neuron of *SI Appendix*, Fig. S4*A*).

Local field potential (LFP) analyses further confirmed that perisaccadic LFP modulations in the deeper (more motor) SC layers were different for different images as the saccade targets, again for metrically and kinematically matched saccades (*SI Appendix*, Fig. S10 *A–D*). LFP modulations also distinguished between real objects and scrambled versions of them (*SI Appendix*, Fig. S10 *E–G*). Thus, as part of the transformation in population representation of images alluded to above (Fig. 3), an increasingly

strong sensory tuning emerged in the most motor SC layers. While we saw this at the time of the motor burst itself, it is interesting to note that other work has revealed a hidden visual sensory response (to target onset) in the most motor SC layers when normal gaze fixation was experimentally disrupted (32).

Saccades toward a Blank Also Alter SC Motor Bursts. Given all of the above, a relevant question to ask is what happens in the extreme case of no visible saccade targets at all? The classic memory-guided saccade paradigm (33, 34) involves just that: A brief cue first indicates the target location; then, after the instruction to trigger an eye movement is issued (by the removal of a fixation spot), a saccade is generated toward a blank. In 2001, Edelman and Goldberg found that some SC neurons stopped emitting motor bursts completely in this case (13). This observation was similar to the ones made earlier by Mohler and Wurtz in 1976, in which they found that some SC neurons did not emit any motor bursts for spontaneous eye movements (5). These neurons, with so-called visually dependent saccade-related (VDSR) motor bursts, were subsequently generally assumed to be a rarity in the SC. However, when investigating memory-guided microsaccades (35), we recently found that up to approximately a fifth or a quarter of microsaccade-related neurons in the rostral SC did not emit motor bursts for microsaccades toward a blank (35). So, we next asked how SC neurons behaved for memory-guided saccades in general and whether it was easy to find neurons with VDSR motor burst properties.

We analyzed a dataset of 114 SC neurons in which monkeys generated vector-matched saccades toward the RF hotspot location under two conditions: with or without a visible white spot. The dataset was the same as that reported in our recent publication on the dissociation between SC motor bursts and saccade kinematics (12), but its presentation in that article was not easy to appreciate from the perspective of the current study. Here, we plotted the neuronal modulation indices of the population as a histogram. The modulation indices were negative when the motor bursts for a blank were weaker than those for a visible spot at the same location (12) (also see the *Inset* equation in Fig. 6*A*). As can be seen from Fig. 6*A*, 76.3% of the neurons (87/114) had a weaker motor burst for saccades toward a blank. Even though the peak velocities of the saccades were also slower in this case (12), thus violating the condition of matched kinematics that we enforced in all of our other experiments above, past work in the literature has shown that the weaker motor bursts for saccades toward a blank were not fully explained by slower peak velocities (12, 13). Therefore, saccades toward a blank are associated with generally weaker SC motor bursts than vector-matched saccades toward a visible spot.

Of course, and as also described in ref. 12, some neurons (about a quarter) actually increased their discharge for saccades toward a blank. This could reflect one aspect of the transformed visual representation at the time of saccade generation that we alluded to above (e.g., Fig. 3), and it warrants further investigation in future studies.

Next, and motivated by the VDSR phenomenon, we inspected the neurons in the lowest quintile of modulation indices from Fig. 6*A*. We found that their motor bursts for saccades toward a blank were drastically reduced or even completely eliminated. Four examples of such neurons are shown in Fig. 6*B*, and an additional four example neurons from the rest of the distribution of Fig. 6*A* are shown in *SI Appendix*, Fig. S11. Thus, SC neurons can exhibit a much larger impact of the absence of a visible saccade target on their discharge than might be accounted for by the slightly slower generated movements.

Finally, we inspected yet another dataset, now from Hafed and Chen (36) and containing more than 400 neurons (again with saccades toward either a spot or a blank). We again found it easy

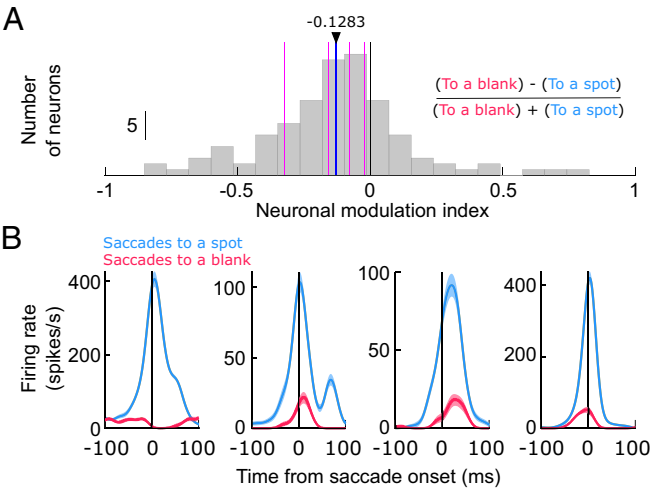

Fig. 6. Dependence of SC neuronal movement commands on the presence of a visual saccade target. (*A*) Distribution of neuronal modulation indices from the database of (12) comparing motor bursts for vector-matched saccades toward either a white spot or blank. The modulation indices were negative if motor bursts were weaker for the blank (see *Inset* equation). More than three quarters of the neurons had negative modulation indices; the thick blue line indicates the population mean (with numerical value indicated above the line). The thin magenta lines indicate the interquintile boundaries. (*B*) Perisaccadic firing rates from four example neurons from the lowest quintile of the distribution in *A* (left of the leftmost thin magenta line). In each panel, the light blue curve shows the average firing rate of a neuron when the monkey made saccades toward a single location, marked by a visible white spot. The light red curve shows the average firing rate of the very same neuron and for the very same saccade vector, but now when there was no visible target. There was a large reduction in motor bursts. See also four additional example neurons from this database in *SI Appendix*, Fig. S11, and six additional example neurons from yet another database in *SI Appendix*, Fig. S12. Error bars: SEM.

to identify neurons with VDSR characteristics, as can be seen from the six example neurons presented in *SI Appendix*, Fig. S12. Thus, an almost complete elimination of SC motor bursts with saccades toward a blank is a robust and relatively prevalent phenomenon in multiple datasets; sensory tuning in SC neuronal movement commands (Figs. 1–5) extends to the case of removing the visual stimulus altogether (Fig. 6 and *SI Appendix*, Figs. S11 and S12).

Relation to V1 Effect in Steady Fixation. Finally, why might there be sensory tuning in SC neuronal movement commands? In seminal work, Sommer and Wurtz (37) reported that SC motor bursts are relayed faithfully to the cortex. Our results imply that, besides the intended saccade vector, SC-sourced corollary discharge can provide a visual preview of the soon-to-be-foveated target, allowing the visual system to bridge a gap of sensory uncertainty caused by rapid eyeball rotation. Indeed, when we simultaneously recorded V1 activity in the same tasks of Fig. 1 (*Materials and Methods*), we found that AUC discrimination performance in SC motor bursts peaked perisaccadically to a level that was at least as good as how V1 neurons discriminated between their most and least preferred peripheral images during steady-state gaze fixation (Fig. 7; the orange SC curves show results from the SC neurons that were recorded simultaneously with the V1 neurons, with consistent results). Thus, during saccades, the SC possesses a reliable sensory representation, which may provide a transsaccadic sensory bridge for perception, exactly when coherent retinal image input is lacking due to rapid eyeball rotations.

Discussion

We observed a robust visual sensory representation embedded within SC neuronal eye movement commands (e.g., Figs. 1 and 2). This representation amplifies weak visual signals (e.g., Fig. 3 *D*–*F*),

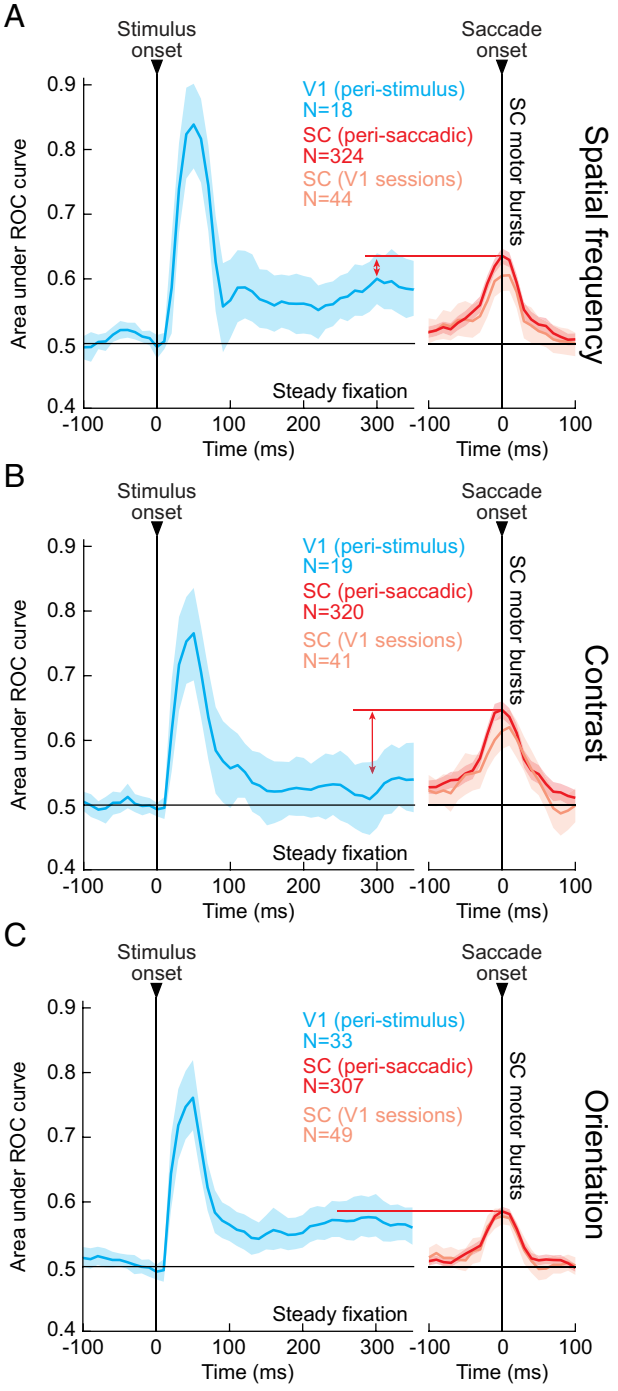

Fig. 7. SC motor bursts as a potential means for providing a transsaccadic sensory bridge of visual information across rapid eye movements. (*A*) We simultaneously recorded primary visual cortex (V1) activity with some of our SC neurons (with overlapping RF locations; *Materials and Methods*). For each V1 neuron, we calculated peristimulus AUC discrimination performance between its most and least preferred images in the visual burst epoch (light blue). After an initial peak in the stimulus-evoked visual bursts, the visual representation in peripheral V1 returned to a lower, but still feature-tuned, baseline during fixation, like in V4 (21, 38). The sensory-tuned perisaccadic SC motor burst signal that we observed (red: all neurons; orange: simultaneously recorded neurons with V1) had AUC discrimination performance (between the most and least preferred images) that peaked to a level similar to how V1 discriminated peripheral images in steady-state fixation. Thus, when the eyes rapidly move and the cortex expects uncertain retinal input, the SC still possesses a sensory representation of the peripheral saccade-target appearance (also see Fig. 3 *G–I*). (*B* and *C*) Similar results for the contrast and orientation image manipulations. In all cases, peak SC perisaccadic AUC discrimination performance was higher than or similar to steady-state AUC discrimination performance of peripheral image information in the visual cortex during fixation. Error bars: 95% CIs.

and it is strong for images of real-life objects (e.g., Fig. 4). It also occurs at a time in which a retinal transfer of visual information about the saccade target ballistically takes place from the periphery to the fovea, causing large afferent sensory uncertainty.

Given that the SC integrates a large amount of visual information from the retina and cortex (23, 39, 40), sensory tuning in its saccade movement commands is an ideal means for internally maintaining evidence about the visual appearance of saccade targets, at a time when such evidence from external afference might be unreliable. Indeed, amplification of weak visual signals during motor bursts fits with a large range of evidence that perception is enhanced at the saccade target around the time of eye movements (24–27). A presaccadic strengthening of feature-tuned neuronal representations in the visual cortex also takes place (38). Interestingly, even though SC visual responses to small spots of light are weak in the retinotopic lower visual field, SC motor bursts for downward saccades to such spots are stronger (12). Thus, amplification of weak SC visual signals might be a general property of this structure's motor bursts.

The results of Fig. 7 also suggest that sensory tuning in SC neuronal movement commands may be more relevant for the SC's ascending pathways to the cortex (41, 42) than for its descending projections to the oculomotor control network. While such ascending pathways have historically been suggested to provide only the vector information of the saccade, to spatially remap retinotopic visual representations (37, 41, 43), sensory tuning in SC motor bursts could allow the same pathways to additionally relay a sensory prediction signal of the peripheral saccade target appearance; such a peripheral preview (even though it is coarser than foveal visual analysis) could be perceptually useful, for example, in predicting the foveal visual sensory consequences of saccades (44), or in bridging transsaccadic perception (45–47). It could also presaccadically enhance perception of the saccade target (24–27) and aid in visual search (48).

If so, then classic perisaccadic perceptual phenomena, such as saccadic suppression (49) and mislocalization (50), which are thought to depend on SC-sourced corollary discharge signals (42, 43, 51, 52), should also be expected to vary with different saccade targets. In other words, if similar saccades toward different images are associated with different SC motor bursts, and if these bursts relay more than just the vector of the saccades via corollary discharge, then perisaccadic phenomena dependent on SC-sourced corollary discharge should also depend on saccade target appearance.

We recently investigated perceptual saccadic suppression with saccades made across backgrounds of low or high spatial frequency (53). Saccadic suppression was significantly stronger for the low spatial frequency condition (53). The saccade targets for the different background images were indeed different images, exactly like in our neurophysiological manipulations here. Therefore, it is indeed plausible that sensory tuning in the SC motor bursts might be linked to modulating the properties of perisaccadic suppression. Similarly, perisaccadic remapping of visual RF locations in the SC, a neurophysiological phenomenon that may be linked to perisaccadic perceptual mislocalization, was also found to strongly depend on the visual context (54).

It would be interesting in the future to further investigate the detailed dependence of perisaccadic perceptual suppression and mislocalization on the visual appearance of the saccade target. This would demonstrate that sensory tuning in SC neuronal movement commands may provide other brain areas with more than just the vector information of executed movements via SC-sourced corollary discharge signals.

We find this idea to also be particularly intriguing from the perspective of postsaccadic foveal visual processing. After every

saccade, foveal neurons, in the SC or in any other visually responsive brain area, suddenly experience a novel image that they did not experience before the eye movement. If SC motor bursts now contain information about the visual appearance of the peripheral saccade target, then this information could be transferred to foveal representations well before visual reafference has materialized. If so, then foveal neurons, in the SC or elsewhere, could receive a trans-saccadic prediction of the target appearance, which could aid in establishing perceptual stability. This idea is testable by recording foveal neuronal activity (say, in the SC) and altering peripheral images intrasaccadically in the middle of an eye movement. In this case, the foveal neurons would experience, via visual reafference, a different image than the peripheral presaccadic image that was present in the environment (but that was outside of the foveal neurons' response fields (RFs)). If these foveal neurons, in turn, had prior predictions about the presaccadic image's features (perhaps via sensory-tuned SC motor bursts), then such neurons might signal a sensory prediction error and mediate a sensation of perceptual change.

It is also intriguing to consider what the most motor neurons of the SC (in the deeper layers) represent. We found that these neurons were still influenced (in their motor bursts) by the visual appearance of the saccade target (e.g., Fig. 5 and *SI Appendix*, Fig. S10). This happened even though the neurons did not really exhibit much visual responses at stimulus onset. Interestingly, when they perturbed gaze fixation via a trigeminal blink reflex induced by airpuffs to the eye, Jagadisan and Gandhi also unmasked a strong visual response in motor neurons (32). This time, the response that they observed occurred to a visual target that appeared right after the blink perturbation, so it was a classic visual response. Thus, there really does seem to be a hidden, latent visual sensory signal even in the deeper, motor SC layers. It would be interesting in future studies to characterize further properties of this signal.

Indeed, there are a multitude of additional future tests to consider as a direct consequence of our results. For example, would there be center-surround interactions when generating a saccade toward the middle of, say, a donut-shaped stimulus with different features inside the middle of the donut hole than around it? Similarly, are there figure-ground interactions, which would give even more functional significance to our real-life object results of Fig. 4? And, what happens when memory-guided saccades are generated based on a memory of an image rather than a small spot of light? Answering all of these questions will help clarify the nature of the sensory representation that is present in the SC at the time of saccade triggering, and it can also help clarify to what extent image salience versus image features per se contribute to modifying SC motor bursts. Finally, it is important to also learn how timing matters in all of this: In other words, what happens if we suddenly remove or change an image right before saccade onset? When before the saccade would the stimulus need to change for the motor burst to be affected?

This question of timing can clarify how the SC representation gets transformed between the visual and motor burst epochs (Fig. 3 *D*–*I*), and how individual neurons alter their preferred features between these two time points. Hints regarding timing already exist in the work of Edelman and Goldberg (13). When studying saccades toward a blank, these authors changed the time at which a stimulus flash could disappear relative to saccade onset. With sufficient time between the disappearance event and the saccade (e.g., >100 to 200 ms), the visually dependent neurons stopped emitting a motor burst. However, with shorter time intervals, the same neurons emitted motor bursts as if the stimulus was still present. This leads us to hypothesize that a stimulus feature can influence SC motor bursts after enough afferent processing delay has passed for the visual signal to be present at the level of the SC (from the retina) by the time of saccade triggering.

Having said all of the above, the SC still contributes to saccade generation. The question now becomes how it does so. Even though it is often suggested that SC motor bursts are critical for saccade control (8, 10, 11), increasing evidence suggests a significantly smaller role, consistent with our observations. For example, SC motor bursts are affected by audio-visual combinations without altered saccades (55). Moreover, saccades toward a blank are often associated with opposite changes in SC bursts and movement kinematics, relative to what happens with saccades toward a visible spot (12, 13). And, on top of that, a substantial fraction of neurons outright stops bursting for saccades toward a blank (Fig. 6 and *SI Appendix*, Figs. S11 and S12) (5, 13, 35). Finally, reward expectation alters all aspects of SC responses in saccade paradigms, including both visual and motor bursts (16). Therefore, SC movement commands can be useful for other aspects of active behavior. Indeed, given that the SC is causally necessary for maintaining visual object representations in a patch of the temporal cortex (56), and given the sensitivity of SC neuronal movement commands to images of coherent visual objects (Fig. 4), it is intriguing to consider the possibility that the SC can influence the temporal cortex also at the time of saccades. This would provide an ideal active vision pathway to the processing of natural visual scenes in normal behavior.

We close with the thought that our results can potentially help resolve some long-standing mysteries about SC neuronal movement commands. For example, population activity spreads across the SC during saccades (57), but no convincing explanation for this exists. Since small spot targets are spectrally broadband stimuli, it could be that perisaccadic spreading activity for such targets is just a manifestation of different spatio-temporal response field properties for images of different spatial frequencies. This, along with investigating whether the SC can causally influence cortical visual feature updating across saccades, will undoubtedly significantly clarify long-lasting mysteries on perception, action, and the self-monitoring internal processes that necessarily link the two.

Materials and Methods

All experiments were approved by ethics committees at the regional governmental offices of Tübingen (under animal experimentation license CIN 4/19G).

We recorded SC activity from two adult, male rhesus macaque monkeys (M and A), aged 8 to 9 y and weighing 9.5 to 10 kg. We also simultaneously recorded V1 activity from monkey A.

Behavioral Tasks. Our primary task was the "Saccades-to-X" paradigm. This was a modified version of the delayed saccade paradigm, but now using an image as the saccade target. A spot was still placed at the image center to ensure similar saccade metrics and kinematics across trials.

In different blocks, we used different series of images. For Saccades-to-Spatial-Frequency, the saccade target consisted of a disc (3° radius), the inside of which was a vertical sine wave grating (100% contrast). In Saccades-to-Contrast, the grating was still vertical, but it now had a fixed spatial frequency (1 cpd). For Saccades-to-Orientation, both the spatial frequency (1 cpd) and contrast (100%) were fixed. Finally, for Saccades-to-Objects, we had images of objects as the eccentric images.

To test the generalizability of our results to immediate, visually guided saccade situations, we designed a second Saccades-to-X paradigm, but now without a forced delay. When the fixation spot was removed, an eccentric gray target appeared simultaneously. The visual feature was now luminance contrast polarity: Targets darker/brighter than the background were defined as negative/positive polarity stimuli (19, 58). Also note that in this task, we did not provide a central

marker spot on the discs, and this was because the discs were already smaller than the other images.

For V1, we ran the Saccades-to-Spatial-Frequency, Saccades-to-Contrast, and Saccades-to-Orientation tasks; the gratings were placed such that overlapping SC/V1 visual RFs were visually stimulated.

Gratings approximately filled SC visual RFs. For simultaneous SC/V1 recordings, this meant larger images than V1 RFs, since we observed that V1 visual RFs were smaller than in the SC. However, the gratings still robustly activated V1 neurons (e.g., Fig. 7).

Eye Movement Data Analysis. We detected saccades using our established methods (59, 60).

To ensure similar saccadic execution across all different image types within a given paradigm, we first ensured that saccade vectors were matched by removing outliers. To further rule out subtle systematic differences between saccades, we then analyzed the movements' metrics and kinematics across image conditions.

To analyze catch-up saccades (*SI Appendix*, Fig. S2), we collected the very first saccade to occur after the primary movement.

Neuronal Data Analysis. Our primary goal was to analyze saccade-related motor bursts. To do so, we defined a motor burst epoch as the time interval between −50 ms and 25 ms from saccade onset. For comparison, we also analyzed stimulus-evoked visual bursts. For classifying SC neurons into different functional cell types, we additionally measured baseline and delay-period activity.

For analyzing SC saccade-related motor bursts, in each task variant (e.g., Saccades-to-Contrast), we defined (for each neuron) the image associated with the strongest saccade-related motor burst as the "most preferred" image. We also defined the image associated with the weakest saccade-related motor burst as the "least preferred" image. Because different neurons had different preferred and nonpreferred images (see *Results*), this classification allowed us to obtain population-level effect sizes across neurons. To do so, we normalized each neuron's firing rate and then averaged across neurons.

We also calculated neuronal modulation indices. The neuronal modulation index was defined as the motor burst strength of the neuron for the most preferred feature minus the motor burst strength for the least preferred feature divided by the sum of the two.

We additionally performed comparisons on raw firing rates, either by plotting the raw measurements directly (e.g., Fig. 2*B*) or by using ROC analyses in a manner similar to other studies (21). Our AUC calculations were similar to those we used recently (31). For Saccades-to-Objects, we were struck by the preference of saccade-related motor bursts to real object images as opposed to scrambles (e.g., Fig. 4*F*). Therefore, we checked whether neurons had significant perimovement AUC elevations when comparing object images to scrambled images.

For LFP analyses, we obtained raw wide-band signals from each electrode contact. We then applied zero-lag filtering as described previously (36). To classify whether an LFP channel was in the more visual (superficial) or more motor (deep) SC layers, we classified each electrode channel's multiunit activity using a visual–motor index (61, 62).

For state-space analyses, we performed a pseudopopulation analysis (20, 63). For each task, the instantaneous firing rate of all neurons that we recorded from was a point in an N-dimensional space of the activity of the population of N neurons. As all neurons' firing rates changed across time (e.g., after stimulus onset or perisaccadically), the population activity representation moved in this N-dimensional space. We, thus, assumed stability across sessions of SC activity since not all neurons in our population were recorded simultaneously (20).

V1 visual response analyses were similar to SC analyses, except that our measurement interval was 30 to 150 ms after stimulus onset.

Additional methodological details are provided in *SI Appendix*, *SI Extended Methods*.

Data, Materials, and Software Availability. The raw SC visual and motor burst data collected for the purposes of this study are publicly available at: https://osf.io/qpj7m/ (64).

ACKNOWLEDGMENTS. We thank Tong Zhang for help in plotting some data from their study. This study was funded by the Deutsche Forschungsgemeinschaft: 1) BO5681/1-1; and 2) SFB 1233, Robust Vision: Inference Principles and Neural Mechanisms, TP 11, project number: 276693517.

1. M. A. Basso, P. J. May, Circuits for action and cognition: A view from the superior colliculus. *Annu. Rev. Vis. Sci.* **3**, 197–226 (2017), 10.1146/annurev-vision-102016-061234.
2. N. J. Gandhi, H. A. Katnani, Motor functions of the superior colliculus. *Annu. Rev. Neurosci.* **34**, 205–231 (2011).
3. D. A. Robinson, Eye movements evoked by collicular stimulation in the alert monkey. *Vision Res.* **12**, 1795–1808 (1972).
4. R. H. Wurtz, M. E. Goldberg, Activity of superior colliculus in behaving monkey. 3. Cells discharging before eye movements. *J. Neurophysiol.* **35**, 575–586 (1972).
5. C. W. Mohler, R. H. Wurtz, Organization of monkey superior colliculus: Intermediate layer cells discharging before eye movements. *J. Neurophysiol.* **39**, 722–744 (1976).
6. D. P. Munoz, R. H. Wurtz, Saccade-related activity in monkey superior colliculus. I. Characteristics of burst and buildup cells. *J. Neurophysiol.* **73**, 2313–2333 (1995).
7. C. Lee, W. H. Rohrer, D. L. Sparks, Population coding of saccadic eye movements by neurons in the superior colliculus. *Nature* **332**, 357–360 (1988).
8. I. Smalianchuk, U. K. Jagadisan, N. J. Gandhi, Instantaneous midbrain control of saccade velocity. *J. Neurosci.* **38**, 10156–10167 (2018).
9. H. H. Goossens, A. J. Van Opstal, Blink-perturbed saccades in monkey. II. Superior colliculus activity. *J. Neurophysiol.* **83**, 3430–3452 (2000).
10. H. H. Goossens, A. J. van Opstal, Optimal control of saccades by spatial-temporal activity patterns in the monkey superior colliculus. *PLoS Comput. Biol.* **8**, e1002508 (2012).
11. D. M. Waitzman, T. P. Ma, L. M. Optican, R. H. Wurtz, Superior colliculus neurons mediate the dynamic characteristics of saccades. *J. Neurophysiol.* **66**, 1716–1737 (1991).
12. T. Zhang, T. Malevich, M. P. Baumann, Z. M. Hafed, Superior colliculus saccade motor bursts do not dictate movement kinematics. *Commun. Biol.* **5**, 1222 (2022).
13. J. A. Edelman, M. E. Goldberg, Dependence of saccade-related activity in the primate superior colliculus on visual target presence. *J. Neurophysiol.* **86**, 676–691 (2001).
14. M. Xu-Wilson, D. S. Zee, R. Shadmehr, The intrinsic value of visual information affects saccade velocities. *Exp. Brain Res.* **196**, 475–481 (2009).
15. R. O. Deaner, A. V. Khera, M. L. Platt, Monkeys pay per view: Adaptive valuation of social images by rhesus macaques. *Curr. Biol.* **15**, 543–548 (2005).
16. T. Ikeda, O. Hikosaka, Positive and negative modulation of motor response in primate superior colliculus by reward expectation. *J. Neurophysiol.* **98**, 3163–3170 (2007).
17. C. Y. Chen, L. Sonnenberg, S. Weller, T. Witschel, Z. M. Hafed, Spatial frequency sensitivity in macaque midbrain. *Nat. Commun.* **9**, 2852 (2018).
18. C. J. Ludwig, I. D. Gilchrist, E. McSorley, The influence of spatial frequency and contrast on saccade latencies. *Vision Res.* **44**, 2597–2604 (2004).
19. T. Malevich, T. Zhang, M. P. Baumann, A. R. Bogadhi, Z. M. Hafed, Faster detection of "darks" than "brights" by monkey superior colliculus neurons. *J. Neurosci.* **42**, 9356–9371 (2022).
20. U. K. Jagadisan, N. J. Gandhi, Population temporal structure supplements the rate code during sensorimotor transformations. *Curr. Biol.* **32**, 1010–1025 (2022).
21. T. Moore, M. H. Chang, Presaccadic discrimination of receptive field stimuli by area V4 neurons. *Vision Res.* **49**, 1227–1232 (2009).
22. C. Y. Chen, Z. M. Hafed, Orientation and contrast tuning properties and temporal flicker fusion characteristics of primate superior colliculus neurons. *Front. Neural Circuits* **12**, 58 (2018).
23. Z. M. Hafed, K. P. Hoffmann, C. Y. Chen, A. R. Bogadhi, Visual functions of the primate superior colliculus. *Annu. Rev. Vis. Sci.*, 10.1146/annurev-vision-111022-123817 (2023).
24. H. Deubel, W. X. Schneider, Saccade target selection and object recognition: Evidence for a common attentional mechanism. *Vision Res.* **36**, 1827–1837 (1996).
25. E. Kowler, E. Anderson, B. Dosher, E. Blaser, The role of attention in the programming of saccades. *Vision Res.* **35**, 1897–1916 (1995).
26. M. Rolfs, M. Carrasco, Rapid simultaneous enhancement of visual sensitivity and perceived contrast during saccade preparation. *J. Neurosci.* **32**, 13744–13752a (2012).
27. L. M. Kroell, M. Rolfs, The peripheral sensitivity profile at the saccade target reshapes during saccade preparation. *Cortex* **139**, 12–26 (2021).
28. C. Y. Chen, A. Ignashchenkova, P. Thier, Z. M. Hafed, Neuronal response gain enhancement prior to microsaccades. *Curr. Biol.* **25**, 2065–2074 (2015).
29. X. Li, M. A. Basso, Preparing to move increases the sensitivity of superior colliculus neurons. *J. Neurosci.* **28**, 4561–4577 (2008).
30. C. Tailby, S. K. Cheong, A. N. Pietersen, S. G. Solomon, P. R. Martin, Colour and pattern selectivity of receptive fields in superior colliculus of marmoset monkeys. *J. Physiol.* **590**, 4061–4077 (2012).
31. A. R. Bogadhi, Z. M. Hafed, Express detection and discrimination of visual objects by primate superior colliculus neurons. bioRxiv [Preprint] (2022), https://doi.org/10.1101/2022.02.08.479583 (Accessed 10 February 2022).
32. U. K. Jagadisan, N. J. Gandhi, Disruption of fixation reveals latent sensorimotor processes in the superior colliculus. *J. Neurosci.* **36**, 6129–6140 (2016).
33. O. Hikosaka, R. H. Wurtz, Visual and oculomotor functions of monkey substantia nigra pars reticulata. III. Memory-contingent visual and saccade responses. *J. Neurophysiol.* **49**, 1268–1284 (1983).
34. S. Funahashi, C. J. Bruce, P. S. Goldman-Rakic, Mnemonic coding of visual space in the monkey's dorsolateral prefrontal cortex. *J. Neurophysiol.* **61**, 331–349 (1989).
35. K. F. Willeke *et al.*, Memory-guided microsaccades. *Nat. Commun.* **10**, 3710 (2019).
36. Z. M. Hafed, C. Y. Chen, Sharper, stronger, faster upper visual field representation in primate superior colliculus. *Curr. Biol.* **26**, 1647–1658 (2016).
37. M. A. Sommer, R. H. Wurtz, What the brain stem tells the frontal cortex. I. Oculomotor signals sent from superior colliculus to frontal eye field via mediodorsal thalamus. *J. Neurophysiol.* **91**, 1381–1402 (2004).
38. T. Moore, A. S. Tolias, P. H. Schiller, Visual representations during saccadic eye movements. *Proc. Natl. Acad. Sci. U.S.A.* **95**, 8981–8984 (1998).
39. V. H. Perry, A. Cowey, Retinal ganglion cells that project to the superior colliculus and pretectum in the macaque monkey. *Neuroscience* **12**, 1125–1137 (1984).

40. C. M. Cerkevich, D. C. Lyon, P. Balaram, J. H. Kaas, Distribution of cortical neurons projecting to the superior colliculus in macaque monkeys. *Eye Brain* **2014**, 121–137 (2014).
41. M. A. Sommer, R. H. Wurtz, What the brain stem tells the frontal cortex. II. Role of the SC-MD-FEF pathway in corollary discharge. *J. Neurophysiol.* **91**, 1403–1423 (2004).
42. R. A. Berman, J. Cavanaugh, K. McAlonan, R. H. Wurtz, A circuit for saccadic suppression in the primate brain. *J. Neurophysiol.* **117**, 1720–1735 (2017).
43. M. A. Sommer, R. H. Wurtz, Influence of the thalamus on spatial visual processing in frontal cortex. *Nature* **444**, 374–377 (2006).
44. L. M. Kroell, M. Rolfs, Foveal vision anticipates defining features of eye movement targets. *Elife* **11**, e78106 (2022).
45. G. W. McConkie, C. B. Currie, Visual stability across saccades while viewing complex pictures. *J. Exp. Psychol. Hum. Percept. Perform.* **22**, 563–581 (1996).
46. B. Bridgeman, A. H. van der Heijden, B. M. Velichkovsky, A theory of visual stability across saccadic eye movements. *Behav. Brain Sci.* **17**, 247–292 (1994).
47. A. Buonocore, O. Dimigen, D. Melcher, Post-saccadic face processing is modulated by pre-saccadic preview: Evidence from fixation-related potentials. *J. Neurosci.* **40**, 2305–2313 (2020).
48. A. Nuthmann, A. C. Clayden, R. B. Fisher, The effect of target salience and size in visual search within naturalistic scenes under degraded vision. *J. Vis.* **21**, 2 (2021).
49. B. L. Zuber, L. Stark, Saccadic suppression: Elevation of visual threshold associated with saccadic eye movements. *Exp. Neurol.* **16**, 65–79 (1966).
50. J. Ross, M. C. Morrone, D. C. Burr, Compression of visual space before saccades. *Nature* **386**, 598–601 (1997).
51. S. Shin, M. A. Sommer, Division of labor in frontal eye field neurons during presaccadic remapping of visual receptive fields. *J. Neurophysiol.* **108**, 2144–2159 (2012).
52. R. A. Berman, W. M. Joiner, J. Cavanaugh, R. H. Wurtz, Modulation of presaccadic activity in the frontal eye field by the superior colliculus. *J. Neurophysiol.* **101**, 2934–2942 (2009).
53. S. Idrees, M. P. Baumann, F. Franke, T. A. Munch, Z. M. Hafed, Perceptual saccadic suppression starts in the retina. *Nat. Commun.* **11**, 1977 (2020).
54. J. Churan, D. Guitton, C. C. Pack, Context dependence of receptive field remapping in superior colliculus. *J. Neurophysiol.* **106**, 1862–1874 (2011).
55. M. A. Frens, A. J. Van Opstal, Visual-auditory interactions modulate saccade-related activity in monkey superior colliculus. *Brain Res. Bull.* **46**, 211–224 (1998).
56. A. R. Bogadhi, L. N. Katz, A. Bollimunta, D. A. Leopold, R. J. Krauzlis, Midbrain activity shapes high-level visual properties in the primate temporal cortex. *Neuron* **109**, 690–699.e5 (2021).
57. D. P. Munoz, R. H. Wurtz, Saccade-related activity in monkey superior colliculus. II. Spread of activity during saccades. *J. Neurophysiol.* **73**, 2334–2348 (1995).
58. T. Malevich, A. Buonocore, Z. M. Hafed, Dependence of the stimulus-driven microsaccade rate signature in rhesus macaque monkeys on visual stimulus size and polarity. *J. Neurophysiol.* **125**, 282–295 (2021).
59. C. Y. Chen, Z. M. Hafed, Postmicrosaccadic enhancement of slow eye movements. *J. Neurosci.* **33**, 5375–5386 (2013).
60. M. E. Bellet, J. Bellet, H. Nienborg, Z. M. Hafed, P. Berens, Human-level saccade detection performance using deep neural networks. *J. Neurophysiol.* **121**, 646–661 (2019).
61. C. Massot, U. K. Jagadisan, N. J. Gandhi, Sensorimotor transformation elicits systematic patterns of activity along the dorsoventral extent of the superior colliculus in the macaque monkey. *Commun. Biol.* **2**, 287 (2019).
62. C. Bourrelly, C. Massot, N. J. Gandhi, Rapid input-output transformation between local field potential and spiking activity during sensation but not action in the superior colliculus. *J. Neurosci.* **43**, 4047–4061 (2023).
63. E. F. Kutter, J. Bostroem, C. E. Elger, F. Mormann, A. Nieder, Single neurons in the human brain encode numbers. *Neuron* **100**, 753–761.e4 (2018).
64. M. P. Baumann, A. R. Bogadhi, A. F. Denninger, Z. M. Hafed, Sensory tuning in neuronal movement commands. OSF. https://osf.io/qpj7m. Deposited 1 September 2023.

PNAS

Supporting Information for
Sensory tuning in neuronal movement commands

Matthias P. Baumann, Amarender R. Bogadhi, Anna F. Denninger, & Ziad M. Hafed

* Ziad M. Hafed
Email: ziad.m.hafed@cin.uni-tuebingen.de

This PDF file includes:

SI Extended Methods

Here, we provide exhaustive details on our experimental and data analysis methods.

Laboratory setup and animal preparation

The animal laboratory setup was the same as that described in our recent work (1). Briefly, each animal was placed in a darkened room ~72 cm from a calibrated and linearized cathode-ray-tube (CRT) display (spanning approximately 30 deg horizontally and 23 deg vertically). We controlled the stimulus presentations and data acquisition procedures using a custom-built modification of PLDAPS (2), interfacing with the Psychophysics Toolbox (3-5) and an OmniPlex data acquisition system (Plexon, inc.).

We prepared the animals for behavioral training and neurophysiological experiments described earlier (1, 6, 7). Briefly, in each animal, we implanted a head holder, to stabilize head position, and a scleral search coil in one eye (8), to allow tracking eye movements with high quality using the electromagnetic induction technique (9). We also implanted a recording chamber centered on the midline and tilted 38 deg posterior of vertical. In monkey A, we positioned the chamber to allow access to the SC in the upper half of the chamber and dorsal portions of V1 in the lower half. SC and V1 recordings were performed in the left hemisphere of monkey A. Monkey M's SC recordings were performed in both hemispheres.

We recorded neuronal activity using 16- or 24-channel linear electrode arrays with 50 μm inter-electrode spacing (V-Probes from Plexon, inc.).

Behavioral tasks

Our primary behavioral task was the "Saccades-to-X" paradigm. This was a modified version of the classic delayed, visually-guided saccade task, with the main difference being that we used an image as the eccentric saccade target rather than just a small spot of light.

Each trial started with the presentation of a white fixation spot (10.8 by 10.8 min arc dimensions) presented at display center. The spot had a luminance of 79.9 cd/m^2, and it was presented over a gray background of luminance 26.11 cd/m^2. After the monkey fixated the spot stably for 300-700 ms, an image was presented at an eccentric location. The monkey was instructed to maintain fixation on the spot even after the onset of the eccentric image. After 500-1000 ms of successful gaze fixation, the central fixation spot was removed, instructing the monkey to generate a saccade towards the center of the eccentric image. To minimize saccade vector variability across trials, which was critical for ruling out metric and kinematic changes in the saccades as the main sources of our results, we always provided a clear visual marker at the center of the eccentric image, which served as an anchor for directing the saccades towards. This marker was superimposed on the eccentric image, and it consisted of a white spot, just like the fixation spot, surrounded by a gray disc (0.54 deg diameter) of the same luminance as the background. The surrounding gray disc ensured that the marker spot was visible irrespective of the background image, allowing us to experimentally control, as much as possible, trial-to-trial variability of the saccades made to the extended images. This was important because saccades can span a range of locations on an extended foveated image (10), complicating the interpretation of whether motor burst changes were due to the image or due to different saccade vectors activating different parts of movement-related response fields (mRF's). In subsequent post-hoc analyses (see below), we further controlled trial-to-trial variability of the saccades, again to rule out a trivial motor variance explanation of our results. The monkey was rewarded for successfully generating a saccade towards the image center within 500 ms from fixation spot offset, as well as for maintaining gaze

on the eccentric image center for an additional 500 ms. The reward amount was always the same regardless of what image was presented on a given trial.

In different blocks of trials, we used different series of images as the eccentric saccade targets. For example, in Saccades-to-Spatial-Frequency, the saccade target image consisted of a disc of 3 deg radius, the inside of which was a vertical, stationary sine wave grating of 100% contrast and a specific spatial frequency. The spatial frequency was randomly picked for each trial from among the following values: 0.5, 1, 2, 4, and 11 cycles/deg (cpd).

In the Saccades-to-Contrast variant of the task, the grating image was still vertical like in Saccades-to-Spatial-Frequency, but it now had a fixed spatial frequency (1 cpd). Across trials, we varied the contrast of the grating from among the following values: 100%, 50%, 25%, 10%, and 0%. Note that the 0% contrast grating had no luminance variation in it at all, but the marker spot (described above) was still visible at its center. Therefore, the 0% contrast condition looked identical to a classic delayed, visually-guided saccade task with a small spot as the saccade target. In fact, we used this condition as our “spot” condition in Results. Also note that because high spatial frequencies are also associated with reduced visibility (due to the contrast sensitivity function) as well as weakened SC visual responses (11), the 11 cpd condition from the Saccades-to-Spatial-Frequency paradigm above was also visually quite similar to a classic spot paradigm; it was thus more like a broad-band stimulus rather than a narrow-band one. This explains some of the neuron preference histograms of early stimulus-evoked visual bursts that are shown in Results (e.g. Fig. 3D, E, visual epoch).

We also ran a Saccades-to-Orientation version of the same task. In this case, both the spatial frequency (1 cpd) and contrast (100%) were fixed across trials. However, the grating could have different orientations. We tested 4 orientations across trials, with the following convention of defining orientation: horizontal was defined as 0 deg, and 45, 90, and 135 deg, respectively, were counterclockwise rotations from horizontal.

For Saccades-to-Objects, we were interested in whether our recent observation of visual object detection in the SC (1) extended to the saccade motor burst epoch. We had images of objects as the eccentric images. Each image was now in a square shape rather than a circular aperture as in the task variants above, and we actually analyzed the motor burst data from the same experiments conducted for our recent work (1). In that work, we only analyzed the visual burst data at image onset; here, we analyzed the saccade motor bursts. In each session, we had a total of seven natural images, one from each of seven object categories: human face, human hand, monkey neutral face, monkey aggressive face, snake, fruit, and artificial object. We also had another seven images with a grid of horizontal and vertical lines in front of them (as if the object was behind a wire mesh); another seven images with the phase information scrambled but the spatial frequency and luminance content unaltered; and another seven images with grid scrambling, or a random reshuffling of the grid locations from the image with the objects behind a grid of horizontal and vertical lines (1). The procedures for obtaining all 28 images were described recently (1), and we used existing toolboxes (12) to equalize the images in terms of luminance and spatial frequency content (1). Thus, in total, the monkey made saccades to one of 28 different images in this version of the paradigm. Across sessions, we generated new images that were not used in the previous sessions.

In all of the above task variants, there was a forced delay between target onset and saccade onset. However, in natural behavior, image onsets might “reflexively capture” saccades immediately, meaning that the visual and motor SC bursts occur much closer to each other in time. Therefore, to test the generalizability of our results to immediate, visually-guided saccade situations, we designed a second Saccades-to-X paradigm, but now without a forced delay. The monkey fixated a central fixation spot. After 600-1500 ms, the fixation spot was removed, and an eccentric gray target appeared simultaneously. We used a new feature dimension in this variant of the task, in order to demonstrate the robustness of the phenomenon of sensory tuning in SC neuronal movement bursts. The feature that we used this time was luminance contrast polarity:

targets darker than the background were defined as negative polarity stimuli, and targets brighter than the background were defined as positive polarity stimuli (13, 14). The targets consisted of discs of 0.51 deg radius, and they had one of three absolute Weber contrasts (10%, 50%, and 100%). Thus, in this Saccades-to-Luminance-Polarity task, we had six conditions: two luminance polarities (dark versus bright), and three Weber contrasts per polarity. Also note that in this task, we did not provide a central marker spot on the discs as in the above tasks, and this was because the discs were smaller than the other images already; we chose such smaller discs to demonstrate that the results from the above experiments were not specific to only larger images. Visual bursts from this task were analyzed in our recent study (14), but saccade-related motor bursts were not inspected.

We collected 50 repetitions per condition per session from the Saccades-to-Spatial-Frequency, Saccades-to-Contrast, Saccades-to-Orientation, and Saccades-to-Luminance-Polarity tasks, and we collected 30 repetitions per condition per session from the Saccades-to-Objects task (because of the increased number of conditions in this task). We typically collected Saccades-to-Spatial-Frequency, Saccades-to-Contrast, and Saccades-to-Orientation within the same session. However, Saccades-to-Objects required dedicated sessions due to the larger numbers of trials that were needed. The Saccades-to-Luminance-Polarity tasks were run, largely, in separate sessions as parts of other experiments, like those described in our recent work (14). Finally, for the V1 recordings, we ran the Saccades-to-Spatial-Frequency, Saccades-to-Contrast, and Saccades-to-Orientation tasks, and in simultaneous recording sessions of both the SC and V1; the gratings were placed such that overlapping visual response fields (RF's) of the recorded neurons were visually-stimulated.

In all cases, we placed the saccade target at our estimated best RF and/or mRF hotspot location of the recorded neurons, and we maintained its position throughout a block. This meant that we ran RF mapping tasks before the main paradigms. These tasks were often the classic delayed, visually-guided saccade task or a fixation variant of it, in which no saccade at the end of the trial was required (1). We sometimes also ran memory-guided saccades (with target location defined by a small spot of light). The primary reason for running these saccades was to check for a dissociation of SC motor burst properties from movement kinematics (15), which was a relevant point to make for the current study. However, we also used results from this dataset here as well for some of our analyses (e.g. Fig. 6 and Fig. S11). Our choice of grating size in the main experiments was to approximately fill classic SC visual RF's at the eccentricities that we tested. For simultaneous SC and V1 recordings, this meant that the grating was larger than V1 RF's, since we observed that V1 visual RF's were smaller than in the SC. However, the gratings still very robustly activated V1 neurons, as seen in Fig. 7 in Results.

Eye movement data analysis

We detected saccades in all trials using our established methods (16, 17).

To ensure that we were comparing neuronal activity with similar saccadic execution across all different image types within a given paradigm (e.g. Saccades-to-Contrast), we first ensured that saccade vectors were matched across the image types of the block before proceeding with any neuronal comparisons. This is because SC movement-related RF's are organized topographically (18, 19); therefore, if one image systematically elicited slightly different saccade vectors from another image, then two different parts of a given neuron's movement-related RF would be activated by the two images, rendering any differences in motor burst strengths trivially explained by a difference in the saccade vectors. As a result, we always first ensured that we were comparing motor bursts for vector-matched saccades across all image manipulations within a given task block. For example, for Saccades-to-Contrast, we collected all saccades for each image contrast. We then binned all vector endpoints of the saccades into a binning grid with 0.5 deg resolution (in each of the horizontal and vertical directions). We only included trials into any subsequent analyses if a given vector bin had saccades from all image types in the blocks (i.e. all

contrasts in the example of Saccades-to-Contrast). In our example of the Saccades-to-Contrast task, if a binning grid location had only saccade vectors from low contrast images but not high contrast images, then this would mean that the saccade vectors for low and high contrasts were slightly different from each other. These saccades were, therefore, excluded from any further analyses. Because we provided a central marker on most images to guide the saccades during the experiments, we still ended up with sufficient trial repetitions for the analyses after the vector matching procedures, as evidenced by the individual example trial rasters shown in Figs. 1, 4 and Figs. S4, S7.

To further rule out subtle systematic differences between saccades to one image type versus another as the trivial explanation of our results, after matching the vectors of the saccades per the above procedure, we proceeded to analyze the movements' metrics and kinematics across image conditions. For metrics, we calculated the direction error and the amplitude error of each saccade. Direction error was defined as the angular difference between the vector of the executed saccade and the vector of the image center relative to fixation; amplitude error was defined as the difference in radial amplitude between the vector of the executed saccade and the radial eccentricity of the image center (the saccade target). For kinematics, we calculated saccadic peak velocity. For a given saccade amplitude (as in our task design), the peak velocity should be relatively constant because of the well-known saccadic main sequence relationship (20) (the monkeys were equally rewarded across trials, so other variables that influence saccade speed, like reward, were equalized). Thus, if the peak velocity is similar for saccades to different image types and the SC motor bursts are very different, then this represents a clear dissociation between SC neuronal activity at the time of saccades from the control of saccade execution, as we and others also observed earlier (15, 21).

To analyze catch-up saccades (Fig. S2), we collected the very first saccade to occur after the primary movement had ended. Some trials did not have any catch-up saccades until the monkey was rewarded. These trials were discarded. For the rest, we calculated the onset time of the first catch-up saccade relative to the end of the primary movement. We also calculated the saccade's amplitude, peak velocity, and direction relative to the direction of the primary saccade. Within each task (e.g. Saccades-to-Contrast), we plotted the distributions of catch-up saccade properties in different colors for the different image features that were tested.

For Saccades-to-Objects, analyses of saccade metrics and kinematics (e.g. Fig. 4D, E and Fig. S9) convinced us that the eye movement properties were already well matched across conditions. Therefore, we analyzed all trials in this task, skipping post-hoc vector matching filters. This was useful because there was a larger number of conditions to run in this task, and because vector matching might have caused severe biases in which images were included or removed as opposed to others in a given analysis.

As we describe in more detail below, we typically grouped trials according to the SC motor burst strength. For example, if a neuron had the strongest motor burst for a high contrast image as the saccade target, we defined this image as the "most preferred image" for the "motor burst". Similarly, if the same neuron had the weakest motor burst for a low contrast image, then this image was the "least preferred image" for the "motor burst". With such classification, we could compare saccade metric and kinematic properties for the most and least preferred trials. Therefore, we also analyzed the saccades of such trials. We always showed full distributions of our data points, and we also included descriptive statistics (e.g. mean or median values). For kinematic comparisons between most and least preferred images, we additionally calculated a kinematic modulation index. This index was defined as the peak speed of the eye for saccades to the most preferred image minus peak speed for saccades to the least preferred image, divided by the sum of peak speeds. Thus, if the kinematic modulation index was zero, it meant that saccade peak speed was the same for trials with the most and least preferred images. For each neuron, we had a kinematic modulation index from its sessions' saccades, which we compared to a neuronal modulation index described below. Note that we often recorded multiple neurons simultaneously. However, since different neurons could have different most and least preferred

images, the saccades used for computing kinematic modulation indices (or for other plots of saccadic behavior) were not necessarily the very same saccades for multiple simultaneously recorded neurons.

Neuronal data analysis

We sorted individual neurons offline using the Kilosort Toolbox (22), followed by manual curation using the phy software. We then proceeded to analyze spike times and firing rates in the different conditions. To obtain firing rates, we convolved spike times with Gaussian kernels of s 10 ms.

Our primary goal was to analyze saccade-related "motor" bursts in the SC. To do so, we defined a motor burst epoch as the time interval between -50 ms and 25 ms from saccade onset, in which we measured average firing rates. For comparison, we also analyzed stimulus-evoked visual bursts occurring immediately after image onset. For those, we defined a visual burst epoch as the time interval between 50 ms and 150 ms after image onset during gaze fixation, and we measured average firing rate in this interval.

For classifying SC neurons into different functional cell types (e.g. visual, visual-delay, visual-motor, or motor), we also had additional measurement intervals. The baseline interval was defined as -100 to 0 ms relative to image onset at trial beginning, and the delay-period interval was 400-500 ms after image onset. Within each task variant that we analyzed (e.g. Saccades-to-Contrast), we classified each neuron as being predominantly visual (exhibiting only stimulus-evoked visual bursts), predominantly motor (exhibiting only saccade-related bursts), visual-motor, or visual-delay (exhibiting visual and saccade-prelude activity but no significant motor activity); see Fig. 5A for examples. To do so, we used the measured firing rates in the four measurement epochs described above (baseline, visual epoch, delay epoch, and motor burst epoch) and computed a non-parametric ANOVA (Kruskal-Wallis). We then determined neuronal class by post-hoc tests at the $p<0.05$ level. Very few well-isolated neurons were not classified into any of the above categories, whether due to low activity levels or other reasons causing the statistical tests to fail. In our population analyses pooling all neuron types, we also included these minority unclassified neurons because inspecting them revealed the same patterns as those of the well-categorized neurons. Also note that we classified neurons separately in each task variant because our primary goal was to ask whether sensory-tuning in SC neuronal movement commands was robust even in neurons with relatively stronger movement-related rather than visual-related activity (e.g. Fig. 5) within any given task. The question of whether SC mRF's themselves are different for different image types is orthogonal to this investigation and requires dedicated mRF mapping sessions with multiple image types (a technically-challenging endeavor due to the numbers of trials required). Moreover, there could be task-related variability in firing rates (e.g. differences in delay-period activity) across different stimulus types. Finally, our neuron classification was highly robust across the different tasks, as evidenced by the similarity of our visual-motor indices (described below) across tasks (e.g. Fig. S10A).

For analyzing SC saccade-related "motor" bursts, in each task variant (e.g. Saccades-to-Contrast), we defined (for each neuron) the image associated with the strongest saccade-related motor burst as the "most preferred" image. We also defined the image associated with the weakest saccade-related motor burst as the "least preferred" image. This was done after the vector-matching procedures described above. Because different neurons had different preferred and non-preferred images (see Results), this classification allowed us to obtain population-level effect sizes across neurons. To do so, we normalized each neuron's firing rate and then averaged across neurons. Normalization was done as follows. In each neuron, we found the peak firing rate occurring either after stimulus onset or around saccade triggering. We then used the larger of the two peaks and subtracted the neuron's baseline activity from it. This constituted our normalization constant. For any firing rate that we wanted to normalize in the neuron's data, we subtracted the neuron's baseline activity from it and then divided by the baseline-subtracted maximal response of the neuron (i.e. by our normalization constant). After obtaining the population saccade-related

motor burst strengths for the most and least preferred images, we plotted the differences between them as well (e.g. Fig. 2A, gray).

We also calculated neuronal modulation indices, similar to what we did with the kinematic modulation indices described above. For each neuron, we plotted the average firing rate curve of the neuron around saccade onset. We then measured the maximum of this curve in the interval from -50 to 25 ms relative to saccade onset, and we did this for either the most or least preferred feature. The neuronal modulation index was defined as the burst strength of the neuron for the most preferred feature minus the burst strength for the least preferred feature divided by the sum of the two. We then plotted the distributions of neuronal modulation indices across neurons in our different tasks. To compare neuronal modulation indices to kinematic modulation indices, we plotted the two indices against each other for each task, and we calculated correlation coefficients. This allowed us to assess whether a large change in burst firing rate in a given neuron (e.g. Fig. 2A) was associated with an equally large change in saccade kinematics or not.

Because we found that the most and least preferred images could be different within a single neuron between the early stimulus-evoked visual burst epoch and the saccade-related motor burst epoch (e.g. Fig. S7A, B), we also repeated the above procedure for the early “visual” epoch of the trials (immediately after image onset during fixation), but after first identifying the most and least preferred images of each neuron in this visual epoch. The normalization of firing rates was not re-done since the above normalization was applied to entire trials and not just the motor burst epochs.

To compare the distributions of preferred features in the early stimulus-evoked visual burst epoch and the saccade-related motor burst epoch (e.g. Fig. 3D-F), we performed χ^2 tests for each image manipulation. We also did this for the reflexive version of the saccade task (Saccades-to-Luminance-Polarity; Fig. S6).

We also performed comparisons on raw firing rates, either by plotting the raw measurements directly (e.g. Fig. 2B), or by using receiver-operating-characteristic (ROC) analyses in a manner similar to other studies (23). We calculated the area under the ROC curve (AUC) as a function of time in either saccade or stimulus-evoked visual epochs. For each trial of the “most preferred” image, we measured instantaneous firing rate at a given point (e.g. near saccade onset), and we did the same for the “least preferred” image. We then calculated the AUC across the distribution of trials at that time point. We repeated this procedure as a function of time, and this gave us time courses of AUC changes relative to either saccade onset or stimulus onset. This procedure allowed us to demonstrate differences in saccade-related bursts despite matched saccade vectors, and it is similar to analyses performed for pre-saccadic elevations in visual cortical neurons of area V4 (23). In some analyses, we also performed AUC analyses as a function of identified cell type. Here, we used the classification of neurons described above and performed the analysis only on neurons within a given functional cell class. We then performed a statistical test to evaluate whether the AUC value at saccade onset depended on cell type (e.g. Fig. 5). Specifically, for each peri-saccadic AUC curve in one task (e.g. Saccades-to-Contrast), we measured the average AUC value in the interval from -20 to +20 ms from saccade onset, and we did this for each classified cell type. Then, we ran a non-parametric ANOVA (Kruskal-Wallis) to assess whether cell type influenced the value of the peak peri-saccadic AUC or not. We then performed post-hoc comparisons between pairs of cell types. Our AUC calculations were similar to those we used recently (1).

For Saccades-to-Objects, we were particularly struck by the preference of saccade-related motor bursts to real object images as opposed to scrambles (e.g. Fig. 4F). Therefore, we checked whether neurons had significant peri-movement AUC elevations when comparing object images to scrambled images. Thus, we grouped all seven image categories into one. This resulted in four groups: real objects, grid-covered real objects, phase-scrambled objects, and grid-scrambled objects. We then checked for significant peri-movement AUC values when comparing real objects to either phase or grid-scrambled categories (or both). We assessed significance, similarly to how

we did it recently for SC visual responses to objects (1). Specifically, we calculated bootstrapped confidence intervals for AUC measures; neurons that had AUC values significantly different from 0.5 at the $p<0.05$ anywhere from times -100 to 100 ms relative to saccade onset were deemed to be significant.

For local field potential (LFP) analyses, we obtained raw wide-band signals from each electrode contact. We then applied zero-lag filtering procedures as described previously (24). Briefly, we used notch filtering to remove the line noise frequency (50 Hz) and its next two harmonics (100 and 150 Hz), and we also kept signals <300 Hz as the LFP band. To classify whether the channel from which we collected LFP's was from the more visual (superficial) or more motor (deep) SC layers, we classified each electrode channel's multi-unit activity (MUA) as being predominantly visual or predominantly motor using a visual-motor index (VMI) (25, 26). Specifically, for each channel, we filtered the wide-band signal using a fourth-order Butterworth band-pass filter (750 to 5000 Hz), and we then rectified the signal before passing it through a second low-pass filter (fourth-order Butterworth) with 500 Hz frequency cutoff. For each condition, we plotted stimulus- and saccade-aligned MUA responses after subtracting the baseline MUA level (defined as the average MUA in the final 200 ms before image onset); superficial channels had stronger visual than motor responses, whereas deeper channels had stronger motor than visual response (25, 26). To quantify this, we measured a motor MUA value and a visual MUA value. These were defined as the average baseline-subtracted MUA in the interval -25 to 25 ms from saccade onset (for the motor MUA measurement) or 30 to 200 ms after image onset (for the visual MUA measurement). The VMI was defined as the motor MUA measurement minus the visual MUA measurement divided by the sum of the two. VMI's larger than zero were more motor than visual (e.g. Fig. S10A).

For state-space analyses, we performed a pseudo-population analysis (27, 28). For each task, the instantaneous firing rate of all neurons that we recorded from was a point in an N-dimensional space of the activity of the population of N neurons. As all neurons' firing rates changed across time (e.g. after stimulus onset or peri-saccadically), the population activity representation moved in this N-dimensional space. We, thus, assumed stability across sessions of SC activity since not all neurons in our population were recorded simultaneously (27). Since population activity likely occupied a much lower dimension than the number of neurons, we performed principal components analysis (PCA) and plotted the population trajectory within the first 3 PCA dimensions. These typically accounted for the majority of the variance of population firing rates (e.g. 70-89%). We used such state-space analysis to first compare visual and motor burst population trajectories and then to check for tuning in the motor bursts. In both cases, we normalized each neuron's firing rate before performing PCA, using the same normalization procedure described above.

To compare visual and motor burst population trajectories in PCA space, we concatenated each neuron's activity in a visual interval (from 0 to 200 ms relative to stimulus onset) with activity in a saccade epoch (from -100 to 50 ms relative to saccade onset). Then, we projected the population activity on 3-dimensional PCA space. This allowed us to assess whether visual and motor SC activity occupied similar or different subspaces (e.g. Fig. 3G).

To check for sensory tuning in the motor bursts themselves, we focused on the peri-saccadic interval only, and we projected SC population activity in this interval, using PCA, for different images as the saccade targets. If there was sensory tuning in the SC population motor bursts, then the population peri-saccadic state-space trajectories should differ as a function of which image was the saccade target (despite the vector- and kinematically-matched saccades) (e.g. Fig. 3H). To quantitatively confirm such difference, we then picked a reference peri-saccadic trajectory from one of the image features of the experiment (e.g. spot in the Saccades-to-Contrast experiment), and we calculated the Euclidean distance of each other image feature's population activity trajectory from this reference trajectory. We did this for times around saccade onset. Moreover, we calculated Euclidean distances from the entire high-dimensional population space, and not just from the 3-dimensional PCA sub-projection of only 3 principal components. For

checking Euclidean distances against a null distance distribution, we performed 1000 permutations in which we randomly picked a reference and a condition trajectory, and we then calculated the Euclidean distance between the two.

Analyses of V1 visual responses were similar to those of SC visual responses, except that our measurement interval was 30 to 150 ms after stimulus onset, since we observed that V1 neurons had slightly earlier visual response latencies than SC neurons.

Finally, in our analysis of memory-guided saccades from past experiments (15), we replotted the same neuronal modulation indices calculated earlier (15) but now as a histogram distribution (Fig. 6A). The modulation indices involved measuring the motor burst for vector-matched saccades towards either a spot or a blank. They were calculated as indicated in the equation in Fig. 6A (15).

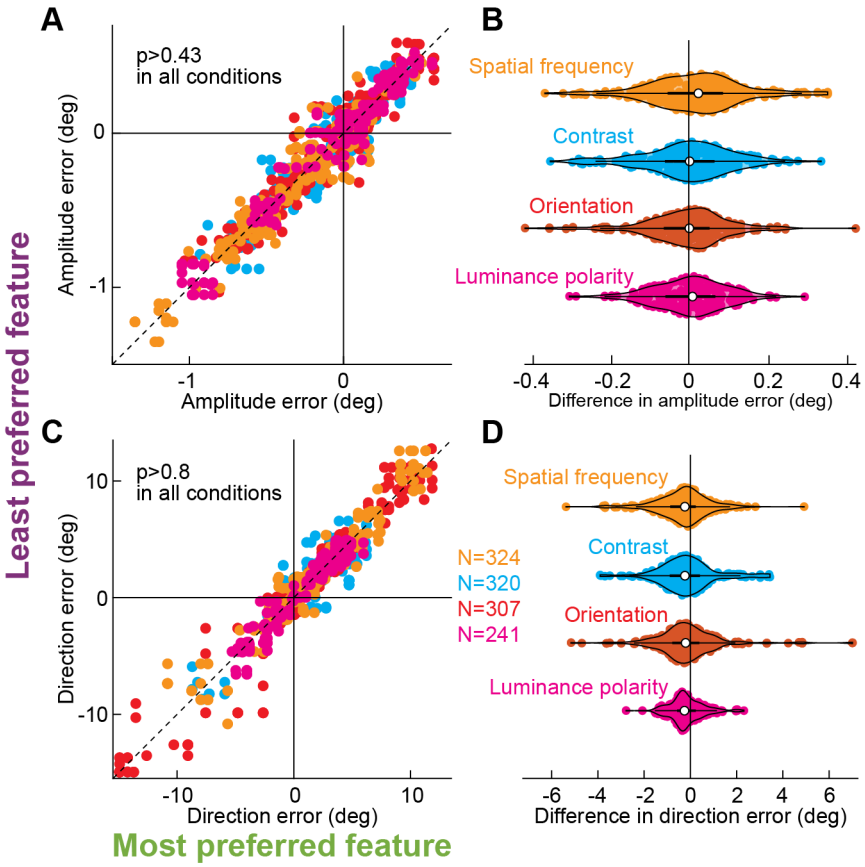

Fig. S1. Independence of sensory tuning in SC neuronal movement commands from eye movement metric properties. (A) For each image manipulation of Fig. 2 (different colors), and for each neuron (individual symbols), we plotted the amplitude error of the saccades to the most and least preferred images of the neuron (based on its motor burst strengths). Despite the large differences in saccade motor bursts (Fig. 2), the amplitude errors were similar across images. This confirms our vector matching procedures (Materials and Methods). P-values indicate rank-sum test results from each image manipulation. **(B)** Distributions of amplitude error differences between most and least preferred image trials from **A**. The violin plots always straddled zero. **(C, D)** Similar observations with saccade direction errors. The numbers of neurons indicated apply to **A**, **B** as well.

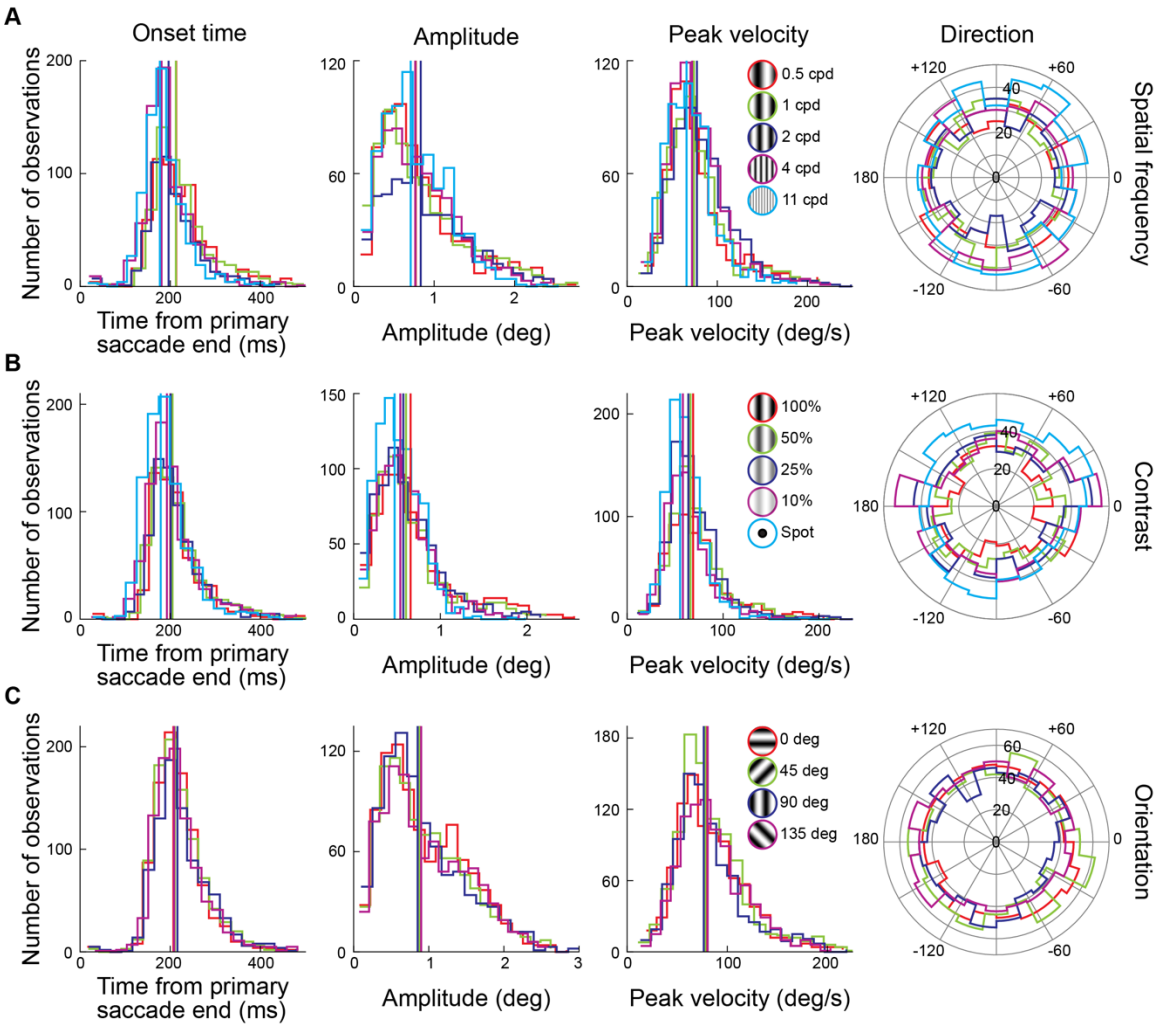

Fig. S2. Independence of sensory tuning in SC neuronal movement commands from the properties of catch-up saccades after the primary movements. (A) For the spatial frequency image manipulation, the leftmost panel shows the distribution of catch-up saccade onset times after the end of the primary saccade. Each color shows a specific image feature towards which the primary saccade was directed. The vertical lines indicate the means of the individual distributions. The second plot shows similar distributions but for catch-up saccade amplitude, and the third plot does it for catch-up saccade peak velocity. The final polar plot shows the distribution of catch-up saccade directions relative to the direction of the primary saccade (that is, a direction of zero in the plot would indicate that the catch-up saccade was in the same direction as the primary saccade). In all panels, the distributions of catch-up saccades were very similar to each other for the different image features, despite the differences in SC motor burst strengths that we observed (Figs. 1, 2). **(B)** Similar observations for the contrast image manipulation. **(C)** Similar observations for the orientation image manipulation. Note that our other tasks (Materials and Methods) also had similar properties of catch-up saccades.

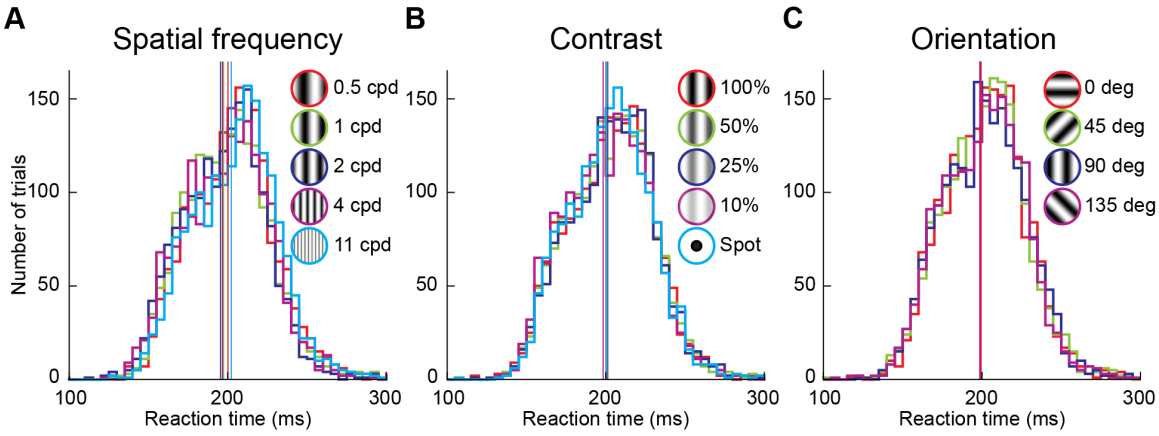

Fig. S3. Independence of sensory tuning in SC neuronal movement commands from intrinsic image salience, as inferred from saccadic reaction times. (A-C) In each of the spatial frequency, contrast, and orientation image manipulations, we used a delayed-saccade paradigm to enforce a period of steady-state gaze fixation between image onset and saccade triggering. This allowed us, as much as possible, to equalize saccadic reaction times across image features within each image manipulation, as can be confirmed from the strongly overlapping saccadic reaction time histograms in each panel. Thus, even though some image features, like low spatial frequencies (11), might be more intrinsically salient than others we equalized this as much as possible by our delayed-saccade paradigm. Note also that in our luminance polarity image manipulation, we used reflexive saccades instead, and the results were unchanged despite strong differences in saccadic reaction times with different image features (see Fig. S4). Vertical lines indicate mean reaction times for each image feature.

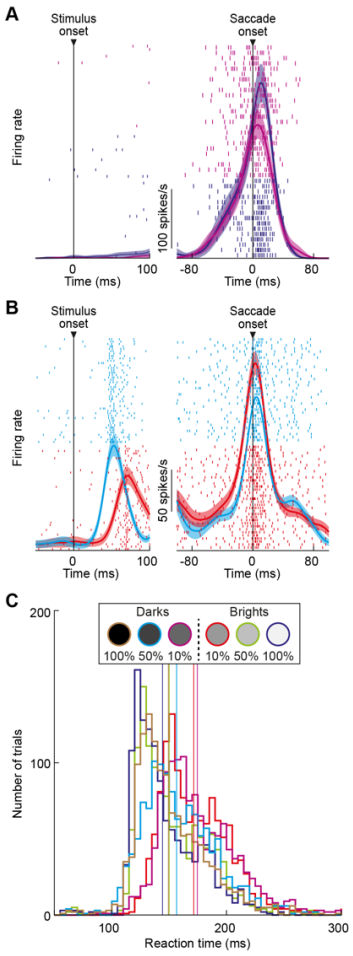

Fig. S4. Independence of sensory tuning in SC neuronal movement commands from reflexive versus delayed saccades. (A) An example neuron's firing rates from our luminance polarity image manipulation. In this image manipulation, we avoided delayed saccades, and the monkeys reflexively looked at the peripheral stimulus as soon as it appeared. This example neuron had almost non-existent visual responses to stimulus onset, but it had strong motor bursts. For two different image features, the motor bursts were very different, similar to the example neuron of Fig. 1. Error bars: 95% confidence intervals, and the numbers of trials are indicated by the number of spike raster rows shown. Other conventions are similar to Fig. 1, and the colors indicate the individual image features, as per the legend in **C**. **(B)** A second example neuron possessing both visual and motor bursts. Note how the visual burst had strongly different latencies from stimulus onset in the two shown conditions, which was also reflected in different saccadic reaction times (**C**). Nonetheless, the motor bursts were still sensory-tuned like in the delayed-saccade paradigm of Fig. 1. Also note how the neuron flipped its image feature preference between visual and motor burst epochs, showing weaker visual bursts but stronger motor bursts for the same image. This is consistent with a transformed SC representation of images at the time of saccade triggering (also see Fig. 3 and Figs. S6-S8). Error bars: 95% confidence intervals, and trial numbers can be inferred from the shown spike rasters. **(C)** With the reflexive saccade paradigm used in this image manipulation, saccadic reaction times strongly depended on image contrast, and there were modulatory effects of luminance polarity (14). Thus, whether saccadic reaction times were equalized (Fig. S3) or not (this figure), sensory tuning in SC neuronal movement commands was still robustly observed. Vertical lines indicate mean saccadic reaction times for each image feature.

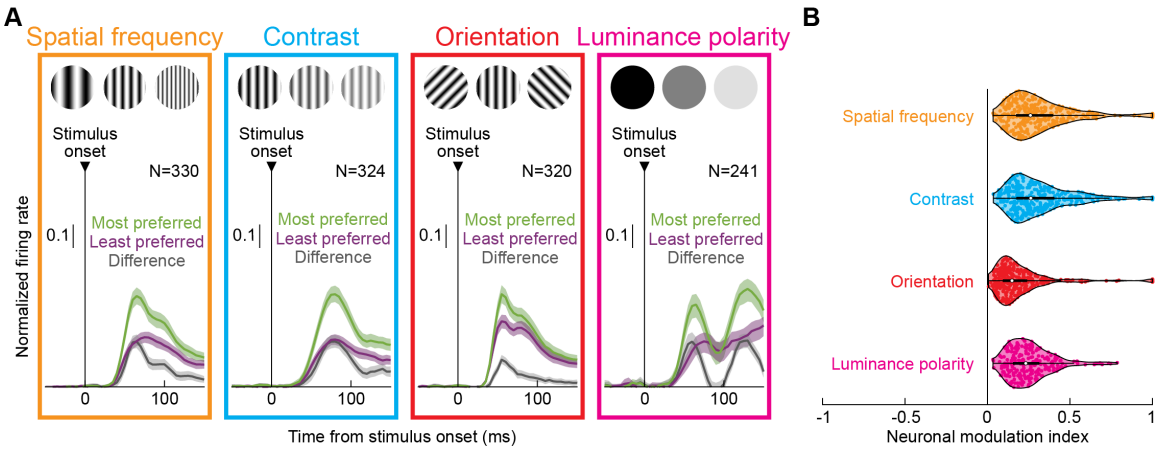

Fig. S5. Sensory tuning in SC visual responses. (A) Analyses like those in Fig. 2A, but for the visual responses of the neurons rather than their activity at the time of saccade triggering. The differences in firing rates between most and least preferred images in the visual bursts were smaller than in the saccade bursts of Fig. 2A, consistent with the AUC discrimination performance results documented in Fig. 3A-C. **(B)** Neuronal modulation indices from the visual burst epoch; these were calculated similarly to the modulation indices in the motor bursts, but based on visual burst measurements and feature preferences (Materials and Methods). All conventions are similar to Fig. 2. Also note that the luminance polarity image manipulation was from the reflexive saccade paradigm. Therefore, there were secondary elevations in firing rates after the initial visual responses in **A**, reflecting the saccade motor bursts. Error bars: 95% confidence intervals, and neuron numbers are indicated in **A**.

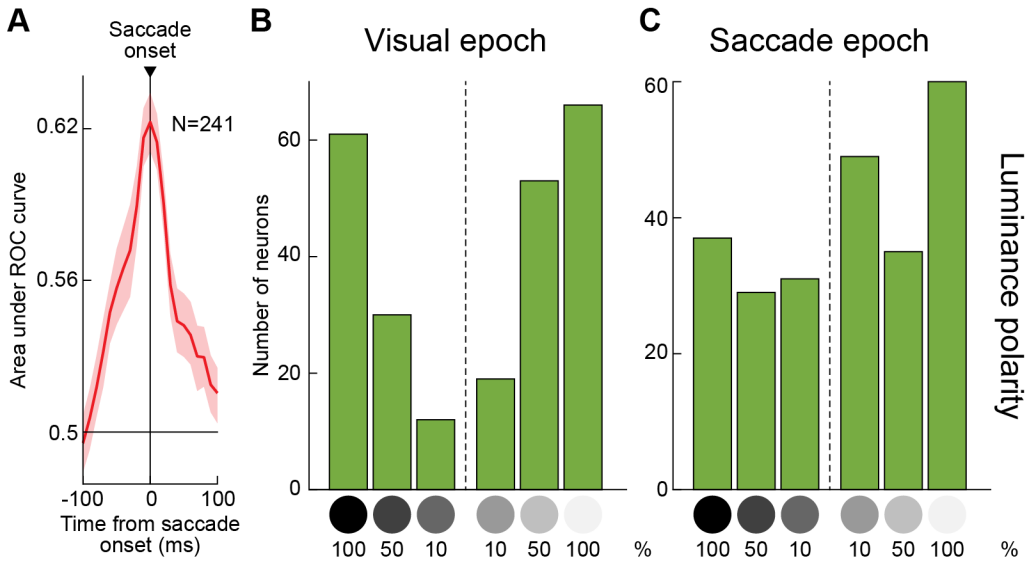

Fig. S6. Similar observations to Fig. 3A-F during the reflexive saccade paradigm. (A) From the luminance polarity image manipulation, we plotted peri-saccadic AUC discrimination performance across neurons. Consistent with Fig. 3 and the example neurons of Fig. S4, there was a peak in AUC discrimination performance at the time of SC motor bursts. **(B, C)** Also consistent with Fig. 3, the distribution of preferred image features at saccade onset (**C**) was broader than that at stimulus onset (**B**), suggesting amplification of weak visual signals at the time of saccade generation even with reflexive, visually-guided saccades. This difference in distributions was statistically significant ($p=7.4 \times 10^{-6}$; $\chi^2=31.4927$; χ^2 test). Figure S4B shows an example neuron with such amplification at the time of saccades. Also see Fig. S8 for high-dimensional population activity trajectories in the reflexive saccade paradigm.

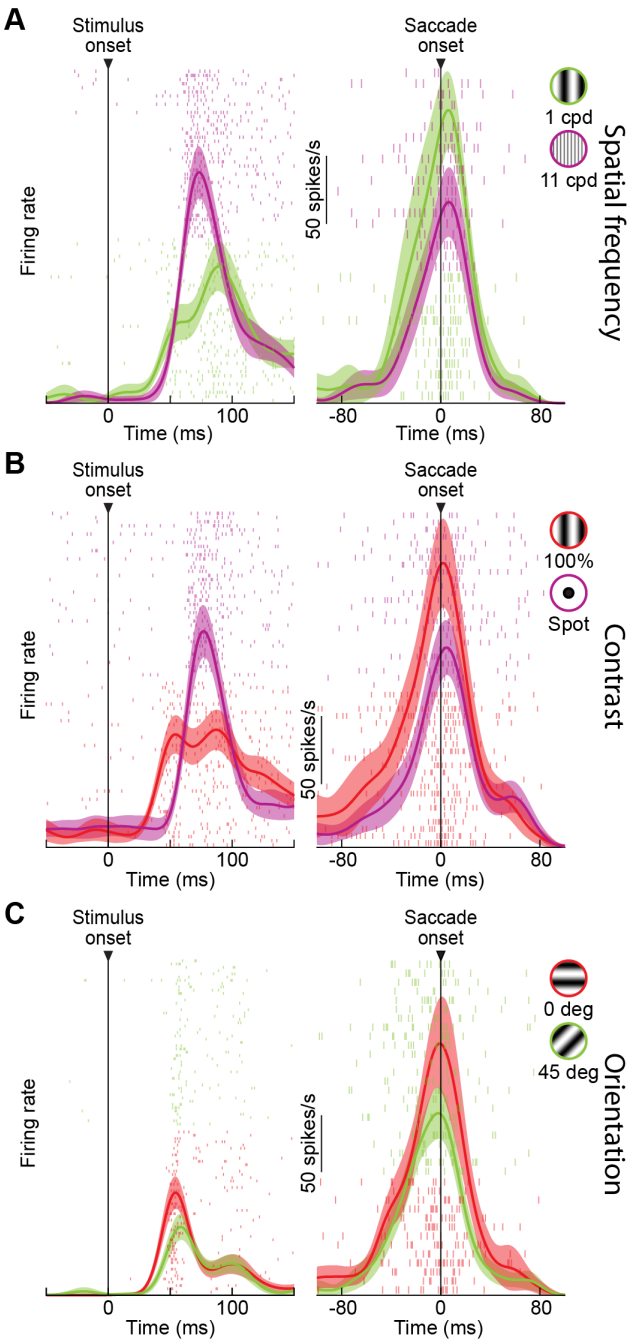

Fig. S7. Potential transformation of image preferences between stimulus and saccade onsets in individual SC neurons. (A-C) Three example neurons from our three image feature manipulations with the delayed saccade paradigm, demonstrating how a changed feature preference can occur between visual and motor epochs with simple grating stimuli. Note how the weak signals in the visual epochs in **A**, **B** were transformed into stronger motor bursts at the time of saccade triggering. Also note that this is similar to the example neuron of Fig. S4B in the immediate, reflexive saccade paradigm. The neuron in **C**, on the other hand, did not exhibit an altered preference between its visual and motor epochs. Error bars: 95% confidence intervals, and trial numbers can be inferred from the shown spike rasters.

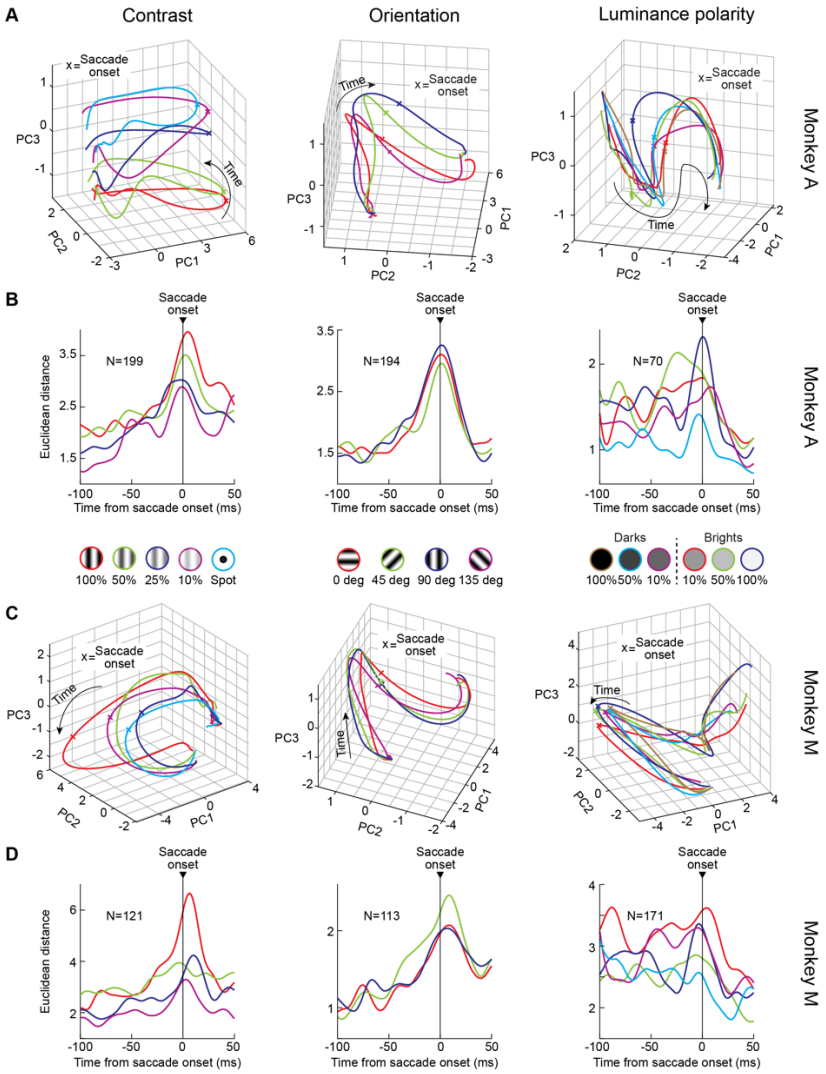

Fig. S8. Embedding of image feature information in SC population activity at the time of saccades. (A) Monkey A population activity trajectories in the first 3 principal components after PCA decomposition in the contrast, orientation, and luminance polarity image manipulations (spatial frequency was shown in Fig. 3H). Consistent with Fig. 3H, SC neurons occupied different manifolds in population activity space at the time of saccade triggering for different image features. Note that in luminance polarity, the saccades were reflexive. Thus, visual and motor bursts occurred in close temporal proximity to each other. Nonetheless, their transformation into quasi-orthogonal manifolds between the visual and motor epochs was still visible, consistent with Fig. 3G. **(B)** For each image manipulation, we picked a reference condition (spot for contrast, 135 deg for orientation, and 100% dark for luminance polarity), and we then plotted the peri-saccadic Euclidean distance of high-dimensional SC population activity from this condition at the time of saccade generation. In each case, the Euclidean distances were different for different image features, suggesting the embedding of sensory information at the time of SC motor bursts (despite vector and kinematic saccade matching). Note that for luminance polarity, the sustained elevation of Euclidean distances before saccade onset reflects the visual epochs of this reflexive saccade task, which were also sensory-tuned. **(C, D)** Similar results from monkey M. Also see Fig. S9D-G for consistent results of sensory tuning in SC neuronal movement commands with real-life object images.

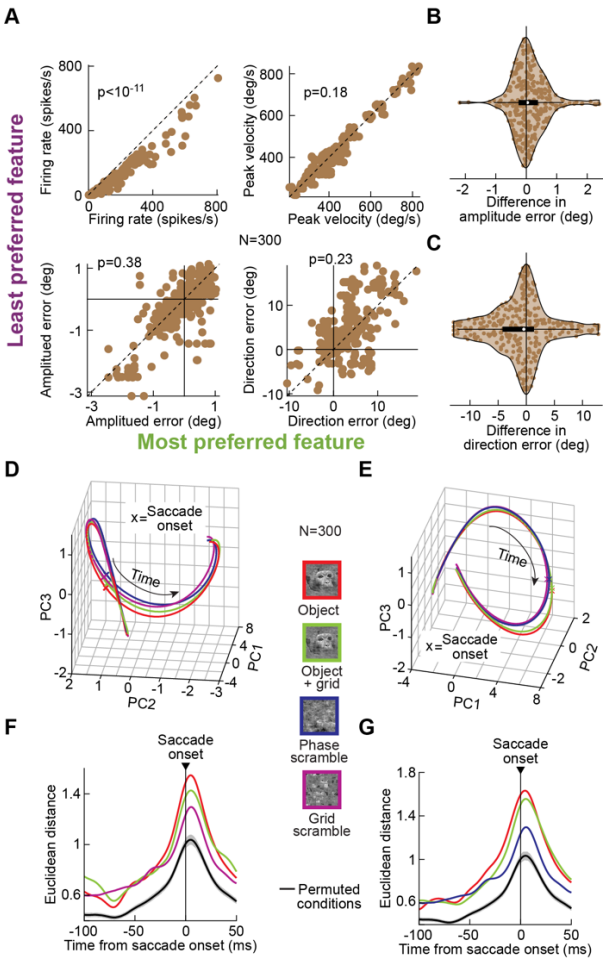

Fig. S9. Real-life object representations in SC neuronal movement commands. (A) Plots similar to Fig. 2B, C and Fig. S1A, C showing a dissociation between motor burst effects between most/least preferred images (top left) and saccade kinematics (top right) or saccade metrics (bottom left and right) in the experiment testing real-life object images (Fig. 4). **(B, C)** Distributions of saccade amplitude and direction error differences between most and least preferred images like in Fig. S1B, D, consistent with the interpretation that SC motor burst differences in this experiment were not explained by systematic differences in eye movement parameters (also see Fig. 4D, E). **(D, E)** Two different views of the peri-saccadic PCA-space population trajectories from both monkeys in the experiments with object images. Note how object and object+grid images (having coherent visual form images within them) were more differentiated from phase-scrambled and grid-scrambled images. **(F)** High-dimensional space Euclidean distances as a function of time from saccade onset when phase-scrambled images were the reference trajectory. This is a similar analysis to that in Fig. 3I, but for the real-life object experiments. Euclidean distances peaked near saccade onset, and they were consistently higher than distances obtained with randomly shuffled reference and non-reference trajectories (black +/- 95% confidence intervals). Object and object+grid images were also more differentiated (higher Euclidean distances) from phase-scrambled images than grid-scrambled images at the time of saccade triggering, consistent with Fig. 4F. **(G)** Similar analysis to **F** but with grid-scrambled images now providing the reference trajectory. Once again, the object and object+grid images were the most differentiated at the time of saccades from grid-scrambled images. All other conventions are similar to **F**. Therefore, whether referencing to phase- or grid-scrambled images, SC motor bursts for real-life objects were most differentiated from those for scrambled images.

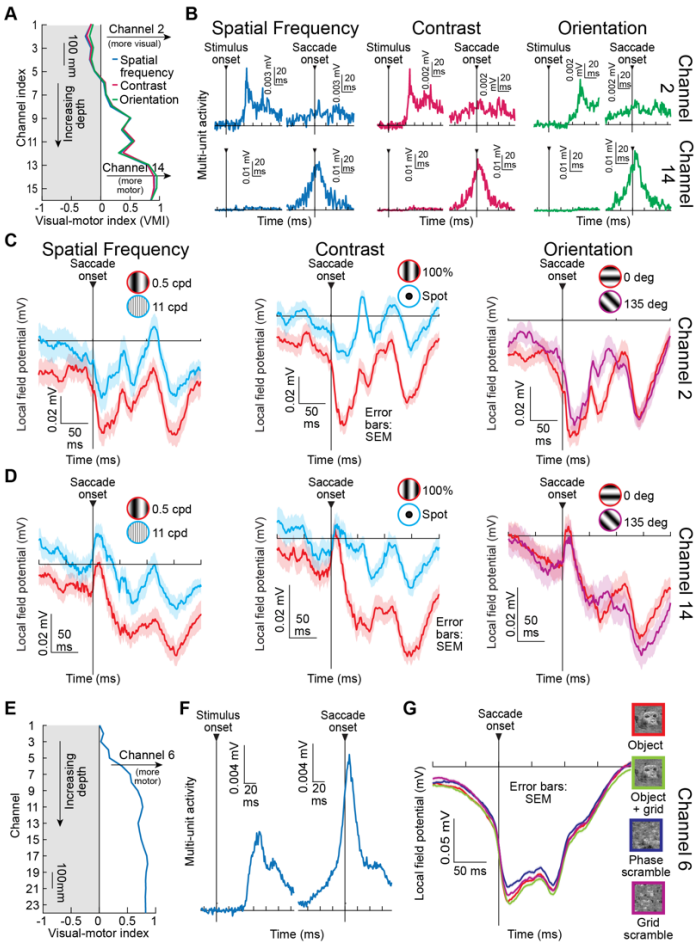

Fig. S10. Embedding of sensory information at saccade onset within the deeper SC layers. **(A)** We calculated a visual-motor index (VMI) (Materials and Methods and refs. 25, 26) across electrode depths from the example session shown in Fig. 1. The VMI, which is inferred from multi-unit activity (MUA) near a given electrode contact, is positive for more motor layers and negative for more visual layers, and the example neuron of Fig. 1 was recorded from channel 14 (that is, from a strongly motor layer). The VMI was calculated for each image manipulation separately (3 colors), and it was robust across them. **(B)** Example MUA activity profiles near stimulus or saccade onset from the same example session. Responses are shown from channel 2 and channel 14, demonstrating how channel 2 was predominantly visual (no motor bursts) and channel 14 was predominantly motor (no visual bursts). **(C)** Local field potential (LFP) profiles around saccade onset for two example features (e.g. 0.5 and 11 cpd) from each image manipulation tested in this session (spatial frequency, contrast, and orientation). The LFP responses from channel 2 are shown. There were differences in peri-saccadic LFP responses for different image features of the saccade targets, despite matched saccade kinematics and metrics. This is consistent with the presence of sensory information in the local SC network at the time of saccade motor burst generation. Note how the effect was weakest for the orientation image manipulation. **(D)** Similar analyses from the deeper motor layer of channel 14 (where the example neuron of Fig. 1 was recorded). There was still a clear sensory signal in the peri-saccadic LFP responses despite the depth of the recording, consistent with the results of Figs. 1-3, 5. Again, the effect was weakest in the orientation image manipulation. **(E-G)** VMI, MUA, and LFP responses from another session from the real-life object experiment. Peri-saccadic LFP responses from an example motor layer (same as that of the example neuron of Fig. 4B) also differentiated between coherent and scrambled object images (**G**). Error bars in all cases: SEM.

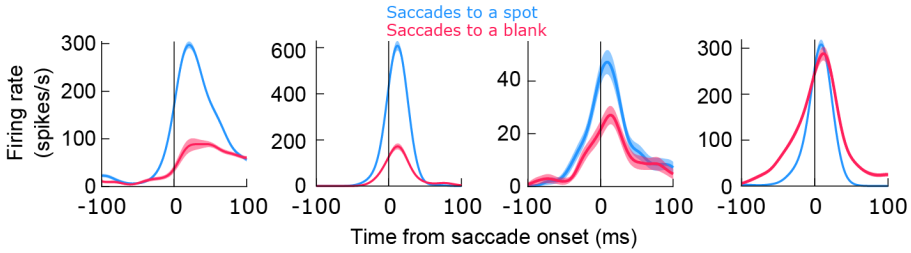

Fig. S11. Comparison of SC motor bursts for saccades made towards either a white spot or a blank. Four additional example neurons from different parts of the distribution of neuronal modulation indices of Fig. 6A. The leftmost two neurons had much weaker peak saccade-related discharge for the blank condition than for the visible target condition. This was the case despite the fact that the neurons emitted strong motor bursts of up to almost 300 or 600 spikes/s peak discharge when the saccade target was visible. The third neuron was less strongly affected by the absence of a visual target for the saccade, and the fourth neuron was even less affected (this example represented a minority in the population, as can be seen from the distribution of Fig. 6A). Error bars denote SEM, and the saccade vectors were always matched between the visible target and blank conditions (15).

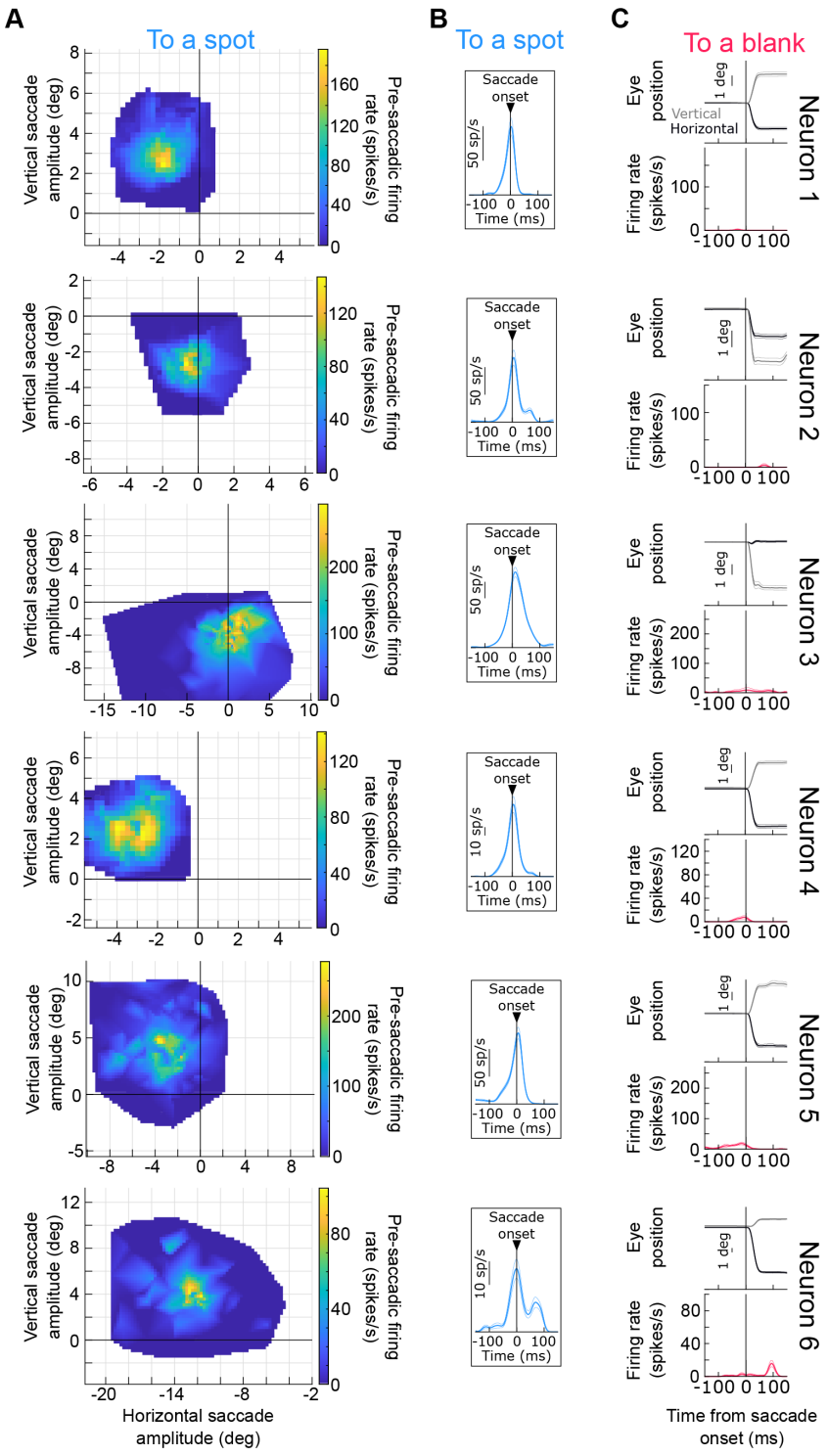

Fig. S12. Example SC neurons with visually-dependent saccade-related discharge from the database of a previous study (24). (A) Each row represents an example neuron in which we plotted the saccade-related motor RF map, from a task in which the saccade target was a white spot. The horizontal and vertical axes indicate horizontal and vertical saccade amplitudes, respectively. The z-axis denotes the average pre-saccadic firing rate (in the final 50 ms before saccade onset) emitted by the neuron. Note that peak motor burst strength typically occurs after saccade onset, suggesting that all six shown neurons had strong motor burst peaks of >100

spikes/s. **(B)** For each neuron, we plotted the average peri-movement firing rate curve from all RF sample locations displayed in **A**. There was a clear saccade-related motor burst. Note that the shown plots under-represent the peak motor burst strength of each neuron because they included all sampled saccade vectors from **A** (including those outside of the RF and with minimal saccade-related discharge). Nonetheless, clear saccade-related motor bursts could still be seen. **(C)** We then plotted each neuron's discharge for a single saccade vector to a location near the RF hotspot location from **A**. This time, the saccade was made towards a blank (memory-guided saccade). Each panel plots the eye position time course (top) and the associated average firing rate (bottom), both aligned to saccade onset. In all six cases, the neurons did not emit motor bursts with saccades towards a blank, despite being clearly saccade-related in **A**, **B**. Error bars: SEM.

SI References

1. A. R. Bogadhi, Z. M. Hafed, Express detection and discrimination of visual objects by primate superior colliculus neurons. *BioRxiv* 10.1101/2022.02.08.479583 (2022).
2. K. M. Eastman, A. C. Huk, PLDAPS: A Hardware Architecture and Software Toolbox for Neurophysiology Requiring Complex Visual Stimuli and Online Behavioral Control. *Front Neuroinform* **6**, 1 (2012).
3. D. H. Brainard, The Psychophysics Toolbox. *Spatial vision* **10**, 433-436 (1997).
4. D. G. Pelli, The VideoToolbox software for visual psychophysics: transforming numbers into movies. *Spatial vision* **10**, 437-442 (1997).
5. M. Kleiner, D. Brainard, D. G. Pelli, What's new in Psychtoolbox-3? (Abstract). *Perception* **36** (2007).
6. J. Skinner, A. Buonocore, Z. M. Hafed, Transfer function of the rhesus macaque oculomotor system for small-amplitude slow motion trajectories. *J Neurophysiol* **121**, 513-529 (2019).
7. K. F. Willeke *et al.*, Memory-guided microsaccades. *Nat Commun* **10**, 3710 (2019).
8. S. J. Judge, B. J. Richmond, F. C. Chu, Implantation of magnetic search coils for measurement of eye position: an improved method. *Vision Res* **20**, 535-538 (1980).
9. A. F. Fuchs, D. A. Robinson, A method for measuring horizontal and vertical eye movement chronically in the monkey. *J Appl Physiol* **21**, 1068-1070 (1966).
10. T. Moore, Shape representations and visual guidance of saccadic eye movements. *Science* **285**, 1914-1917 (1999).
11. C. Y. Chen, L. Sonnenberg, S. Weller, T. Witschel, Z. M. Hafed, Spatial frequency sensitivity in macaque midbrain. *Nat Commun* **9**, 2852 (2018).
12. V. Willenbockel *et al.*, Controlling low-level image properties: the SHINE toolbox. *Behav Res Methods* **42**, 671-684 (2010).
13. T. Malevich, A. Buonocore, Z. M. Hafed, Dependence of the stimulus-driven microsaccade rate signature in rhesus macaque monkeys on visual stimulus size and polarity. *J Neurophysiol* **125**, 282-295 (2021).
14. T. Malevich, T. Zhang, M. P. Baumann, A. R. Bogadhi, Z. M. Hafed, Faster Detection of "Darks" than "Brights" by Monkey Superior Colliculus Neurons. *J Neurosci* **42**, 9356-9371 (2022).
15. T. Zhang, T. Malevich, M. P. Baumann, Z. M. Hafed, Superior colliculus saccade motor bursts do not dictate movement kinematics. *Commun Biol* **5**, 1222 (2022).
16. C. Y. Chen, Z. M. Hafed, Postmicrosaccadic enhancement of slow eye movements. *The Journal of neuroscience : the official journal of the Society for Neuroscience* **33**, 5375-5386 (2013).
17. M. E. Bellet, J. Bellet, H. Nienborg, Z. M. Hafed, P. Berens, Human-level saccade detection performance using deep neural networks. *J Neurophysiol* **121**, 646-661 (2019).
18. D. A. Robinson, Eye movements evoked by collicular stimulation in the alert monkey. *Vision Res* **12**, 1795-1808 (1972).
19. D. L. Sparks, C. Lee, W. H. Rohrer, Population coding of the direction, amplitude, and velocity of saccadic eye movements by neurons in the superior colliculus. *Cold Spring Harb Symp Quant Biol* **55**, 805-811 (1990).
20. B. L. Zuber, L. Stark, G. Cook, Microsaccades and the velocity-amplitude relationship for saccadic eye movements. *Science* **150**, 1459-1460 (1965).
21. J. A. Edelman, M. E. Goldberg, Dependence of saccade-related activity in the primate superior colliculus on visual target presence. *J Neurophysiol* **86**, 676-691 (2001).
22. M. Pachitariu, N. A. Steinmetz, S. N. Kadir, M. Carandini, K. D. Harris, Fast and accurate spike sorting of high-channel count probes with KiloSort. *Advances in Neural Information Processing Systems (NIPS 2016)* **29** (2016).
23. T. Moore, M. H. Chang, Presaccadic discrimination of receptive field stimuli by area V4 neurons. *Vision Res* **49**, 1227-1232 (2009).

24. Z. M. Hafed, C. Y. Chen, Sharper, Stronger, Faster Upper Visual Field Representation in Primate Superior Colliculus. *Curr Biol* **26**, 1647-1658 (2016).
25. C. Massot, U. K. Jagadisan, N. J. Gandhi, Sensorimotor transformation elicits systematic patterns of activity along the dorsoventral extent of the superior colliculus in the macaque monkey. *Commun Biol* **2**, 287 (2019).
26. C. Bourrelly, C. Massot, N. J. Gandhi, Rapid Input-Output Transformation between Local Field Potential and Spiking Activity during Sensation but not Action in the Superior Colliculus. *J Neurosci* **43**, 4047-4061 (2023).
27. U. K. Jagadisan, N. J. Gandhi, Population temporal structure supplements the rate code during sensorimotor transformations. *Current Biology* **32**, 1010-1025 (2022).
28. E. F. Kutter, J. Bostroem, C. E. Elger, F. Mormann, A. Nieder, Single Neurons in the Human Brain Encode Numbers. *Neuron* **100**, 753-761 e754 (2018).